1-1-2007

Performance analysis of solar-powered wireless visual sensor network and its applications

Xiaoming Fan
Ryerson University

Recommended Citation

PERFORMANCE ANALYSIS OF SOLAR-POWERED WIRELESS VISUAL SENSOR NETWORK AND ITS APPLICATIONS

By

Xiaoming Fan

M.A.Sc. in Electrical Engineering,
Chinese Academy of Sciences, 1998
P.R.China

A thesis
presented to Ryerson University
in partial fulfillment of the
requirement for the degree of
Master of Applied Science
in the Program of
Electrical and Computer Engineering

Toronto, Ontario, Canada, 2007

UMI Number: EC53699

INFORMATION TO USERS

The quality of this reproduction is dependent upon the quality of the copy submitted. Broken or indistinct print, colored or poor quality illustrations and photographs, print bleed-through, substandard margins, and improper alignment can adversely affect reproduction.

In the unlikely event that the author did not send a complete manuscript and there are missing pages, these will be noted. Also, if unauthorized copyright material had to be removed, a note will indicate the deletion.

UMI®

AUTHOR'S DECLARATION

I hereby declare that I am the sole author of this thesis.

I authorize Ryerson University to lend this thesis to other institutions or individuals for the purpose of scholarly research.

Author's signature:___

I further authorize Ryerson University to reproduce this thesis by photocopying or by other means, in total or in part, at the request of other institutions or individuals for the purpose of scholarly research.

Author's signature:___

BORROWER'S PAGE

Ryerson University requires the signatures of all persons using or photocopying this thesis. Please sign below, and give address and date.

Name	Signature	Address	Date

ABSTRACT

Performance Analysis of Solar-Powered

Wireless Visual Sensor Network and Its Applications

© Xiaoming Fan 2007

Master of Applied Science

Department of Electrical and Computer Engineering

Ryerson University

This thesis discusses the performance of a solar-powered wireless visual sensor network and its visual applications. We examine the performance of a layered clustering model in sparing communication energy consumption and prolonging the system lifetime. The experimental result illustrates that the system can transmit the same amount of video packets with less energy consumption when video quality is at achievable minimum distortion rate. Therefore, the visual sensor network may achieve higher performance by applying rechargeable solar cell and layered clustering. After receiving all the video data, the sink may be applied with advanced post-processing techniques. We propose an innovative post-processing algorithm, Parallel Self-Organizing Tree Map (PSOTM) that can be implemented in the sink. By means of processing visual data in parallel, PSOTM may achieve faster image segmentation with insignificant impacts on the visual quality.

ACKNOWLEDGMENT

PUBLICATION LIST

CONFERENCE PAPERS

1. X. Fan, J. Randall, and I. Lee, "Image Segmentation Using Parallel Self Organizing Tree Map", *Proceedings of IEEE International Conference on Multimedia & Expo*, Toronto, Canada, pp.1905 - 1908, July 2006.

2. C. Wang, X. Fan, M. Du, B. Elder, X. Tang, and L. Guan, "Special Effects in Film Making With Object Based Transformations", *Proceedings of IEEE International Conference on Multimedia & Expo*, Beijing, China, July 2007.

3. X. Fan, W. Shaw, and I. Lee, "Layered Clustering for Solar Powered Wireless Visual Sensor Networks", accepted by *IEEE International Symposium on Multimedia* 2007.

TABLE OF CONTENTS

VIII

LIST OF FIGURES

LIST OF TABLES

CHAPTER 1

INTRODUCTION

1.1   Motivation and Objectives

In the past several decades, advances to information technology (IT) have provided much support to economic growth around the world. Recently, in the IT field, wireless visual sensor networks (WVSNs) and their visual applications, such as, video surveillance, sensing rooms, smart conference rooms, environmental monitoring, military application, disaster management, image segmentation, video processing, etc, have drawn a lot of attention [1][2]. WVSNs are often deployed in unattended environments or open areas like national parks and battlefields, thus leaving the sensors requiring self-management. Due to the limited dimensions of the sensor nodes, the capabilities of most deployed nodes are restricted, especially in processing unit and battery energy. At present, many researchers put emphasis on either prolonging the system lifetime or improving the capability of the sensor nodes, especially central processing unit (CPU). However, improving the capability of the sensor nodes generally leads to the increase of their energy consumption. Hence, the lifetimes of sensor nodes are shortened in the case of equal energy capacity, vice versa. To sum up, only improving one aspect is often at the expense of solving the deadlock between increasing the capability of the sensor nodes and lengthening the system lifetime.

In this thesis, our research focuses on a heterogeneous solar-powered wireless visual sensor networks (HSPWVSNs). Typically, the normal HSPWVSNs are composed of

three components: normal visual sensor node, cluster head node, and base station. Normal visual sensor nodes are equipped with surveillance cameras. Once visual sensor nodes are activated by certain events, the cameras module will be initialized to capture visual signal, encode and transmit video data to the cluster heads. In addition to the function of capturing the video data, the cluster head nodes also have the functions of aggregating, encoding the data from the visual sensor nodes, and forwarding to the base station. Generally, the base stations have larger energy capacity, faster computing speed and more communication resources. They act as a gateway between sensor nodes and the end user. The visual data gathered from the wireless visual sensor network is saved in the sink. The sink can process the video data with post-processing algorithm. The algorithm we proposed in this thesis is Parallel Self-Organizing Tree Map (PSOTM). In this work, we put our focus on:

- How to prolong the system lifetime and improve visual quality of WVSNs at the same time?

- How to improve the image processing performance of the sink in WVSNs?

To solve the above questions, in this thesis:

- We examined the performance of layered clustering and data aggregation models in the solar-powered WVSNs. We also applied video distortion and solar cell modules to the system model of sensor nodes.

- We proposed a novel post-processing image segmentation algorithm, PSOTM to improve image processing performance of the sink.

1.2 Thesis Organization

The thesis is composed of five chapters and the rest four chapters are organized as below. Followed the introduction on Chapter 1, Chapter 2 introduces the related work of WSNs, WVSNs, and image processing techniques, SOM and SOTM.

Chapter 3 examines the performance of a layered clustering model in the WVSNs. Since the energy requirement of visual sensor nodes in WVSNs are much higher than that in VSNs, we applied layered clustering model and rechargeable solar cell unit to the WVSNs. The experiments are implemented under considerations of visual quality and solar cell recharging. The experimental result proves that the layered clustering model can prolong the system lifetime of solar-powered WVSNs in most situations.

Chapter 4 proposes a novel post-processing image segmentation algorithm, PSOTM, which can be applied in the sink. Through processing image in parallel, the algorithm can dramatically improve the image segmentation efficiency with insignificant impact on the image segmentation results.

Chapter 5 provides conclusions and directions for the future work. We first summarize and list our contributions in the thesis. Then future work on the homogeneous and heterogeneous solar-powered WVSNs is provided.

CHAPTER 2

RELATED WORK

This chapter introduces the related work of WSNs, WVSNs, SOM, and SOTM. The remainder of this chapter is organized as follows,

Section 2.1   introduces related work of WSNs. It includes five sub-sections: solar cell, routing improvement, lifetime and topology, quality of service, and energy and routing.

Section 2.2   introduces related work of WVSNs. It includes two sub-sections: visual quality, and energy and topology.

Section 2.3   introduces related work of image processing techniques. It includes two sub-sections: SOM, and SOTM.

2.1   Wireless Sensor Networks

WSNs consist of numerous spatially distributed autonomous tiny sensors that communicate with wireless [75][76]. They are used to capture the signals, such as temperature, humidity, sound, wind speed, vibration, air pressure, motion detection, and pollutants strength, at different locations. The military application such as battlefield surveillance is the original motivation of the sensor network [79]. Later, the applications of wireless sensor networks are employed in many civilian application areas, including

4

atmosphere and home monitoring, healthcare applications, house automation, traffic organization, distance areas monitoring, industrial product monitoring, inventory managing, monitoring patients, assisting disabled patients, virtual keyboard, finding the parking space, smart office, Global Positioning System and etc [77].

Generally, a wireless sensor node is composed of sensing unit, transceiver unit, processing unit, and power unit. According to each node's role and the area size of the WSNs, the dimension of sensor nodes can vary from dust size to book size. The cost of the nodes also varies from several cents to thousands dollars. Consequently, the constraints on the node's cost and size lead to the constraints on the node's components, such as, processing speed, energy capacity, memory size, and the wireless availability.
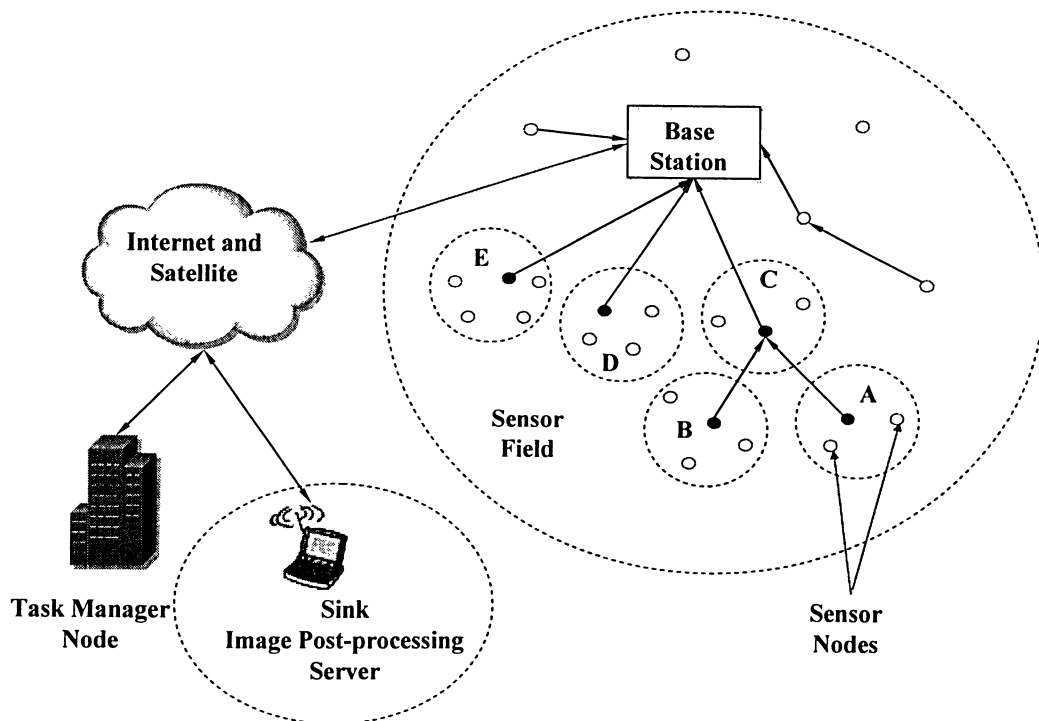
Figure 2.1 Wireless Sensor Networks Architecture
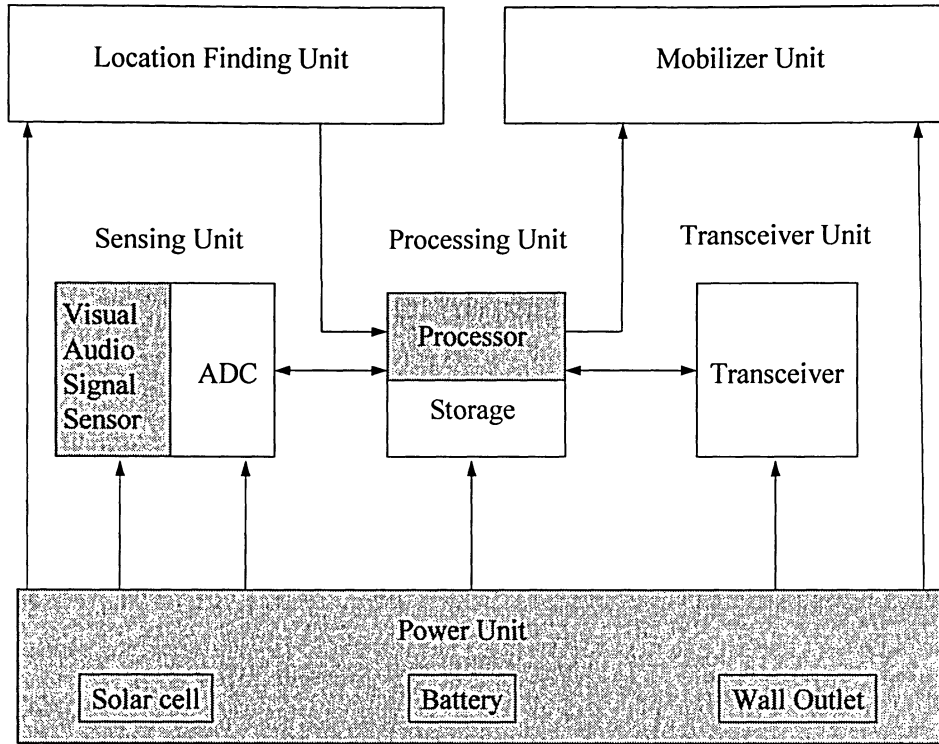
Figure 2.2 Sensor Node Components [81]

WSNs can be classified into two broad types: homogeneous and heterogeneous sensor networks [16][18]. In the homogeneous sensor networks, all the sensor nodes are identical in terms of processing speed, battery capacity and hardware complexity. In the heterogeneous sensor networks, two or more different types of nodes with different energy capacities and functions are used [78]. In general, a heterogeneous WSN is made up of numerous wireless sensor nodes that are randomly distributed in an open area. As illustrated in Figure 2.1, normal sensor nodes are responsible for capturing and generating the signal, processing data and communicating with the other nodes or the base station. The sensors are supposed to own the capabilities of self-organizing, event-detection, even event-activation. Commonly, in a clustering heterogeneous WVSN, base station and cluster heads have relatively stronger processing capability. For a normal sensor node in

6

WSNs, it has a CPU, memory and short-range wire/wireless communication facility and it is universally powered by battery, wall-outlet or solar cell. Figure 2.2 illustrates the structure of a typical visual sensor node [81]. The function descriptions of all the units in the sensor nodes can be found in the Table 2.1.

Unit Name	Function Description
Sensing Unit (Sensor, ADC)	Sensor captures and generates data. The data of visual sensor also includes visual signals. ADC (Analog-to-Digital Converter) converts analog data to digital data.
Processing Unit (Processor, Storage)	Processor processes and encapsulates the data from the sensing unit. Instead of Microcontroller, visual sensors may need digital signal processor (DSP) to process the image or video. Storage stores the operating system of the sensors and data generated by sensing unit or received from other nodes.
Power Unit	Provides the energy to all the units in sensors, the power sources can be battery, solar cell, wall outlet, etc.
Transceiver Unit	Communicates with the other sensors. It includes the components for transmitting, such as antenna, receiver.
Mobilizer Unit	Let the sensors move in the open area.
Location Finder Unit	Let the sensors find their location.

Table 2.1 Wireless Sensor Nodes Components

Compared to the ad-hoc wireless networks, the number of sensor nodes in a sensor network can be several orders of magnitude higher than the nodes in an ad-hoc network. In addition, the topology of a sensor network may change much more frequently. Thirdly, sensor nodes mainly use a broadcast communication paradigm, whereas, most ad-hoc networks are based on point-to-point communications. Fourth, sensor nodes are limited in power capacity, computing speed and memory size. Last, sensor nodes might not have global ID because of the large amount of sensors.

In WSNs, there are five common issues: (1) energy unit that is recharged by solar panel; (2) routing improvement; (3) system lifetime extension and topology revision; (4) quality of service; and (5) energy and routing. We will discuss the related work on these five issues in the following sections.

2.1.1 Solar Cell

Among the energy sources available for scavenging, solar radiation is one of the most profuse energy sources. Solar cell is also one of the very common natural power choices. Moreover, it is compact and compatible with our other energy sources. Compared to other energy harvesting techniques, it is also a well-developed technology. There are numerous prior researchers having worked on advancing solar cell techniques. Particularly, the question of how to avoid false terminating the solar cell recharging procedure is one of common issues. Specifically, for the recharging systems that detect overcharging only by immoderate decline of the charging current or voltage, sometimes the solar panels will cease charging even when the solar cells have not hit their maximum capacities. Abnormal climates, such as thunderstorms, rain, cloudy, or a shade on the solar panel, may cause a dramatically decrease of charging voltage or current that might

lead to a false termination of recharging procedure. Boico *et al.* proposed a method to inhibit the end of solar cell recharging procedure under conditions where the solar cell has not hit its maximum energy capacity [3].

Warneke et al. put forward a compact autonomous design of solar-powered sensor node whose dimension is smaller than $16mm^3$ [4]. The signal of sensor can be transmitted over a bi-direction long distance optical link, which allows it to be used in a one-to-many network configuration. Raghunathan *et al.* further developed a prototype of wireless embedded system that is powered by solar cell and presented four key issues arise from the system design [5]. The four issues are: (1) the solar energy supply is not stable and charging time varies due to the various weathers; (2) battery self-discharge and round trip efficiency; (3) the different solar cell's voltage-current characteristics; (4) the question of how to modulate system's power consumption by selectively deactivating some sub-components. The authors investigated the key issues in the design of solar-powered wireless sensors and embedded systems. Both of the papers discussed the solar-powered sensor node designs and gave the charging rate of solar cell under the conditions of outdoor bright sunlight and indoor illumination.

Since different cities are located in different geographical locations, their daytime tables are also varying. The daytime tables of all main cities around the world in a year can be found on the website [6]. In the thesis, we studied the performance of solar-powered wireless visual sensors in different locations by applying their daytime tables. Furthermore, in the experiment, we also discussed the false termination of recharging procedure. By applying the method of Boico *et al.* [3], the solar cell recharging model is modulated under an ideal condition that is exclusive of false termination in charging procedure.

2.1.2 Routing Improvement

In WSNs, numerous researchers evaluate the performance of routing protocols by employing the existing routing protocols under the same conditions. Mohan *et al.* evaluated the performance of the multi-hop routing protocols in a testbed where the sensors are densely spaced. The authors concluded that HSN DSDV and Reliable Time Sync can achieve higher performance than the other routing protocols in the testbed [7]. Pham *et al.* also presented a comparison of four other wireless sensor network protocols: MultiHopRouter, TinyAODV (Ad-hoc On-demand Distance-Vector), GF (Greedy Forwarding), and GF-RSSI (Greedy Forward with Received Signal Strength Indication) [8]. Performance measurement is conducted on a wireless sensor network testbed for medical application research. Based on the measurements, GF-RSSI performs well in various operating conditions. Especially, it shows a high success rate of packet delivery and moderate energy consumption.

Some researchers improve the system performance by revising the existing routing protocols, such as, AODV and Pulse. Some specific values or weights, such as, path value, and location information have been applied to the existing routing protocols. Gwalani *et al.* proposed AODV-PA, AODV with path accumulation [12]. By evaluating AODV-PA, DSR, and AODV protocols in packet delivery ratio, normalized routing load, and end-to-end delay of data packets, the authors conclude that AODV-PA has a higher performance in most cases, especially in high load scenarios. In addition to the work of Gwalani, Ooi *et al.* proposed AODV-bis, a path accumulation AODV with location information [9]. The difference between AODV and AODV-bis is that AODV-bis uses location information in route discovery. That means the source nodes only forward RREQ to the nodes that are closer than the destination nodes. Compared with transmitting packets from the source nodes to the destination nodes, only sending the packets to the

closer nodes consumes less energy. Thus, the revised protocol spares the transmission energy and bandwidth when the source nodes periodically update their routing tables.

The sensors at standby state can save substantial energy than that at active state. Awerbuch *et al.* proposed an amended Pulse routing protocol by applying periodic pulse routing updating and letting the sensor periodically wakeup [13]. Such a protocol can increase delivery rate and save energy at the same time. For those large-scale networks, the recurrent routing updating consumes the most bandwidth. Zheng *et al.* proposed AODV-Clustering, which is AODV based clustering routing protocol [14]. The clustering algorithm can solve the scalable problem for AODV in the large mobile networks. AODV-Clustering performs better than AODV in the Average Route Acquisition Latency, Quick Route Discovery Mechanism and reduces the RREQ flooding at the cases of large quantity of nodes and heavy load.

Some researchers improve system performance by applying two routing protocols to different segments of a hierarchical sensor network. Bai *et al.* proposed a hierarchical routing model, WPR(Way Point Routing) [10]. The inter-segment routing is DSR and the intra-segment routing is AODV. The advantage of applying these two routing protocols is explained as follows. If an intermediate sensor is malfunctioned or a link is broken, instead of updating all the links in the network, the routing algorithm only updates the segment that has the malfunctioned sensor or broken link. Thus, the algorithm can spare the energy of sensors that are functional and with normal wireless links. This model is especially efficient in the dense wireless networks, for example, over 1000 nodes. In the paper, the authors also proved the protocol has better performance than the other flat routing protocols, such as DSR and AODV, and hierarchical routing protocols, such as CGSR and ZRP, in the large networks.

Some researchers proposed new routing protocols to improve the performance of wireless

sensor network. Yuasa *et al.* proposed a sustainable routing protocol considering easy node exchangeability. [11]. The experimental result shows that the system lifetime can be prolonged with the routing protocol. Marwaha *et al.* also proposed an original routing scheme, Ant-AODV that is the combination of a distributed topology discovery mechanism and AODV routing protocol [15]. The experimental result shows that Ant-AODV can provide better performance than AODV.

2.1.3 Topology and Lifetime

There are also numerous papers discussed on the question of how to prolong system lifetime by improving the network topology in WSNs. Some researchers proposed to generate the system topology by the capabilities of sensors. Chan *et al.* discussed the hierarchical routing protocols in terms of the energy usage, packet latency, and security at the presence of node compromise attacks [16]. The authors also proposed a method to design the network with particular energy, latency and security demands. Yong *et al.* further investigated the generation of a hub-spoke heterogeneous network topology that is adaptively formed according to the resources of the sensor nodes [17]. A protocol named Resource Oriented Protocol (ROP) was developed to build the network topology. This protocol chiefly divides the network operation into topology formation phase and topology update phase. The network is composed of three types of sensors, SRC (Small Resource Capacity), MRC (Medium Resource Capacity), or LRC (Large Resource Capacity).

In heterogeneous wireless sensor networks, the sensors with higher capability can work as cluster heads or base station; the sensors with lower capability can work as normal sensors or range sensor. Du *et al.* proposed a heterogeneous design, incorporating a

mixture of sensors with widely varying capabilities [18]. In the design, a small number of powerful high-end sensors, and a large number of low-end sensors were deployed. The authors also proposed a Cluster Head Relay (CHR) routing protocol for the heterogeneous sensor network. CHR proves its better performance by comparing with two popular sensor network routing protocols: Directed Diffusion and SWR [29]. Additionally, Madan *et al.* analyzed the network lifetime by applying partially and fully distribution algorithm [19]. Under the consideration of limited node energy, the experimental result deduces that the partially distributed algorithm is faster than fully distributed algorithm in rate of convergence. An unequal clustering model that can be applied to the sensor network is proposed by Soro *et al.* [22]. The areas of the layers are derived from the energy functions of the cluster heads in the different layers. By varying the areas of the clusters, the numbers of sensor nodes in the clusters also varies. The authors concluded that with the proposed model, the energy of all the cluster heads can be exhausted synchronously.

Some researchers proposed to divide the network into different segments and assign the sensors different functions or statuses. Vaidya *et al.* developed an innovative video sensor network framework [20]. It is made up of several zones. Each zone includes event-driven sensors, sonar sensors, and visual sensors. Based on the computation of direction and speed of the mobile object, the intelligent sensor management system can activate the cameras in the corresponding area. The system structure is depicted as follows.

- Layer 1: Gateway. A sensor node with more computational power and resources.

- Layer 2: Event driven sensors. This layer is responsible for activating corresponding layer 3's sensors.

- Layer 3: Range sensors. Sonar sensors are responsible for detecting object's position. The sonar sensors can only get the radial distance between object and

sonar sensor.

- Layer 4: Camera and acoustic sensors.

Instead of assigning the heterogeneous sensor nodes into different zone, Yamasaki *et al.* presented an energy-efficient WSN with three models: i) censoring sensors, ii) on-off sensors, and iii) censoring and on-off sensors [21]. For energy saving purpose, the authors recommended the model iii. Proved by the experiment in the paper, the authors can design very energy-efficient WSNs by using censoring and on-off sensors.

2.1.4 Quality of Service

In WSNs, many applications of wireless sensor network require the sensor nodes deliver signal content with a certain level of quality of service (QoS). In the research field on wireless sensor network, the topic on minimizing the energy consumption has attracted many researchers so far. However, the question of how to efficiently deliver application-level QoS, and the question of how to map their wireless transmission requirements to the metrics such as latency and jitter become primary concerns in mainstream research on sensor networks. Biagioni *et al.* proposed a reliability layer that is based on the protocol, MOR (multipath on-demand routing) [23][85]. It incorporates a redundant routing in every node, where the redundant routing can be correlated, not like MDSR [82], AOMDV [83]. Compared with AODV and DSR, the proposed model, MOR that is applied with reliability layer, proves to have better performance in delivering the same quantity data. By applying the QoS value to the existing protocols, it is easy to let them have QoS function. In order to solve the errors that arise from unreliable and poor communication, Mansouri *et al.* proposed Simple Transport Protocol for Wireless sensor network (STPW) [26]. It consists of two parts, one is transport layer method, which is

used to overcome the poor wireless communication, and other is path redundancy, which is used to guarantee the packets delivery.

On the other hand, some researchers enhance the existing routing protocols by adding the QoS weight. Gerasimov *et al.* proposed an end-to-end QoS enhanced AODV routing protocol [24]. By comparing the QoS-AODV with other two similar AODV protocols, the authors concluded that QoS-AODV is more likely to find QoS end-to-end route in the wireless network. Similarly, Zhang *et al.* proposed a routing protocol, QS-AODV, which is the combination of the AODV and QoS value [25]. Comparing with AODV, it can dramatically improve the packet delivery rate in a heavy-traffic MANET with a slight delay.

2.1.5 Energy and Routing

In WSNs, due to restricted dimension of the sensor, the limited energy capacity of the sensor nodes is always the bottleneck on prolonging the system lifetime. Nevertheless, discovering the most reasonable route is an energy consuming task for every wireless sensor node. Many researchers try to find the most efficient way to establish a finest route between normal sensor node and base station. Gomes *et al.* proposed OPER (On-Demand Power-Efficient Routing) that is improved from AODV [27]. OPER-PE (Path Energy) and OPER-NE (Node Energy) are two route selection parameters. Compared with some existing routing protocols, such as, MAER, MBCR, Direct Diffusion, AODV, the proposed routing protocol can spares the energy in finding routes. Moreover, Heeseok *et al.* proposed a routing protocol by applying energy-aware and multipath routing on Nano-Qplus Platform [28]. In the proposed routing protocol, the nodes with higher energy value can be selected during establishing a routing path from source node to

destination node. Energy efficiency is improved and data transmission rate is promoted. Furthermore, Tian *et al.* proposed SWR (single path with repair) that can automatically find an alternative route when there is a break in the single path route [29]. The authors also proved the SWR had better performance than the existing protocols, such as, SWOR, DISJ2, MESH in the delivery rate and average energy consumption per data delivery.

Some researchers implement the routing protocol with energy aware value. Tan *et al.* proposed PAW-AODV (Power-Aware) routing protocol [30]. The authors proved the protocol can deliver more data packets than AODV in the same experiment setup. Additionally, Kim *et al.* proposed an enhanced AODV protocol by applying the energy value [31]. By implementing AODV and enhanced AODV, the system applied later routing protocol proves to have a longer network lifetime than the system applied former routing protocol. Hong *et al.* also proposed an energy-aware routing protocol that is applied in the space exploration [32]. The energy value is regarded as a reference value in the multi-path routing protocol. The result proves the energy-aware load balance routing had the best performance in extending the system lifetime.

2.2   Wireless Visual Sensor Networks

Generally, a WVSN is made up of numerous sensors equipped with visual data collection modules. For a visual sensor node, the sensing unit can capture the visual data; the process unit may need DSP to process the visual data; the power unit has stronger power supply to provide the energy for the visual facility. Besides the functions that WSNs already have, WVSNs have the visual applications, such as:

- **Security:** WVSNs can be the residence surveillance systems. For example, visual sensor nodes can be placed close to the driveway, monitoring and recording the

16

pedestrians, transmitting the video and audio data to the sink. The data can provide the critical clue on the criminal investigation.

- **Industry Control Monitoring:** In the noxious environments, such as the automobile painting, visual sensors can gather visual data on the painting quality.

- **Traffic monitoring:** In highway area, wireless visual sensors can monitor the real time highway traffic; help drivers avoid the traffic congestion.

- **Remote Medicine:** In a desolate area, sensors can transmit the images or video of the patients to the doctors who are in the city. By analyzing the visual data and monitoring the patient on heart beat, pulse, body temperature, blood pressure, doctors can provide the emergency cure and give the prescription [84].

- **Climate Monitoring:** Sensors can continually provide the video data on the climate, such as, cloud, sunrise, sunset, moon, thunderstorm, and rain.

- **Battlefield Surveillance:** For battlefield surveillance, visual sensors can monitor the moving of enemy; provide the location of attack targets, and even the status of battles in a big picture.

- **Shopping Mall:** In the shopping mall, visual sensors can be placed at the entrance. They provide manager of the mall the video data for customer statistic on the shopping habits.

- **Airport Surveillance:** Monitor the registration desk, luggage delivery, plane arrival or departure, and customer density; help the operator to run the airport smoothly.

2.2.1 Visual Quality

In wireless visual sensor networks, the visual applications are the key issue of the normal sensors. Sparing the energy consumption on the one hand and yet guaranteeing the image quality that system requires on the other hand, are two vital facts for wireless visual sensor network. Based on the Rate-Distortion (R-D) model, He *et al.* developed the Power-Rate-Distortion (P-R-D) analysis framework by extending the power value to the R-D model [34]. The power consumption is divided into two parts, power consumption of data transmission (P_t) and power consumption of video coding (P_s). The model has been applied in two scenarios, small and large delay video systems. He *et al.* also introduced concept "accumulative visual information" (AVI) to measure the amount of visual information collected in the VSNs [35]. Besides the entropy, it includes the image distortion, encoding efficiency and energy consumption. Since the old rate-distortion is evolved from the wired network, it can not be applied to WVSNs. He *et al.* proposed a model that includes integrated resource-distortion analysis framework by considering the new resource constraints, such as transmission bandwidth and storage space [36]. By applying the new R-D model, the overall performance of the system can be promoted. Besides the work of He *et al.,* Chow *et al.* also investigated the relationship between image quality and energy consumption [37]. It shows that in the case of long-distance (many hops) transmission, it is better to aggregate the overlapping part of images to decrease the packet's size. However, in the case of short-distance transmission, it might not work so effectively.

2.2.2 Energy and Topology

Numerous researchers put focus on energy economization by optimizing the sensor

location, video flow, and system layout. Kim *et al.* developed a cooperative relaying architecture that reduces the transmitting and receiving energy [39]. The system is made up of three layers, sensor, cluster head and base station. The video sensors are organized as cluster and the cluster heads aggregate the video in the cluster. This proposal is working perfect in high rate video sensor networks. On the other hand, Pan *et al.* believed that the location of base station plays an important role in prolonging the lifetime of sensor networks [41]. Since the communication distances between the sensors and base station are related with energy consumption, the authors proposed two schemes, one is a centralized location-based scheme, and the other is distributed AoA-based scheme. In additional, Chu *et al.* proposed a distributed attention mechanism [42]. It is made up of three layers, pre-attentive, attentive and cognitive layer. The lower level image processing is running on the pre-attentive layer, the attentive layer can be regarded as tracking layer. Furthermore, Obraczka *et al.* investigated on the question of how to manage the information flow in the WVSNs [40].

2.3 SOM/SOTM

2.3.1 Self-Organizing Map

Currently, there are two common topics in the image field, one is image segmentation and the other is image recognition. Researchers have taken great efforts to develop new technologies for image segmentation and recognition [43][44][45]. In early years, only human beings were capable of doing most image segmentation projects. However, the high expense and low efficiency of such manual work are always issues in image

processing. The questions of how to segment a picture intelligently and how to improve the efficiency of segmentation software synchronously are two most popular issues. Recent research has made for suitable self-driven image segmentation technologies to be available in the near future.

T. Kohonen briefly introduces the Self-Organizing Map (SOM) and the applications in his survey paper [47]. Recently, SOM has been used in speech recognition, robotics, process control, and telecommunications applications. However, it performs poorly in various pattern recognition tasks unless manual supervision is possible.

The SOM can also be applied in data visualization and exploration. After considering the different clustering SOM approaches, Vesanto *et al.* proposed a hierarchical agglomerative and partition-based clustering using k-means [48]. In a two-stage procedure, the second stage uses the prototypes generated by the first stage. Accordingly, the proposed algorithm may achieve good performance and shortened processing time.

Dittenbach *et al.* proposed a novel neural network model, growing hierarchical self-organizing map [49]. During an unsupervised training process, the neural network model can migrate into a hierarchical structure. Through application scenarios from the information retrieval area, the proposed algorithm proves to be extremely useful.

2.3.2 Self-Organizing Tree Map

H. Kong, J. Randall, and L. Guan *et al.* investigated the Self-Organizing Tree Map (SOTM) that is a special algorithm derived from SOM with tree building hierarchy [46][33]. SOTM automates the process of determining the correct number of centroids. SOTM maps from a high dimensional Euclidean space [50] onto a finite set of prototypes,

and this technique has been applied on various image processing applications, such as restoration, compression, and segmentation [51]. Furthermore, in image segmentation, the SOTM computing method is employed to attain not only the feature points, but also the centre vectors of feature points. It has proved its classification abilities in performing image segmentation and feature point grouping in the image processing.

SOTM has been applied in many applications. The SOTM has been used for grey level image segmentation and two dimensional data mapping, demonstrating its ability to perform unsupervised data clustering [33]. Moreover, the SOTM has also been applied into automated interactive retrieval tasks in order to minimize user participation [38].

SOTM has sprouted several derived algorithms for applications on content based image retrieval and biofilm image analysis. In CBIR systems, Jarrah *et al.* used the invariance properties of Hu's seven moment invariants for relevance identification [52]. Based on their simulation, an innovative ranking function in the structure of the SOTM is also proposed. Furthermore, Kyan et al. investigated use of the self-organizing feature map (SOFM) with different combinations of other image statistics [80]. The authors applied the model to 3-D microscope image data to automatically enhance and extract biomaterials of interest. In a sample application, this technique allowed for improved level of detail and clear isolation of chromosomes from their background. In further work applied to the area of biofilm segmentation, the SOTM was further enhanced by Kyan *et al* by refining the competitive search strategy. This move made the SOTM more sensitive to the regional associations of different microbial matter thereby improving the segmentation algorithm [53][54]. In this work, Kyan et al also proposed a criterion of refined stop. Consequently, the dynamically generated number of classes becomes more data dependant.

CHAPTER 3

WIRELESS VISUAL SENSOR NETWORKS

This chapter first introduces the background knowledge of WVSNs. Then, layered clustering model and its experiment are illustrated respectively. The remainder of this chapter is arranged as follows,

Section 3.1   introduces the background knowledge of WVSNs.

Section 3.2   presents system model, which is made up of five units, solar cell unit, event trigger unit, energy consumption unit, layered clustering unit, and video distortion unit;

Section 3.3   shows the experiments of the layered clustering model under the considerations of visual quality and solar cell recharging.

Section 3.4   summarizes the layered clustering model for the solar-powered WVSNs.

3.1   Background

Recently, WSNs have drawn a lot of attention in environmental monitoring, military applications, disaster management, etc [1][2]. Due to the restricted item size of the normal sensors, the capabilities of most deployed sensors are limited, typically in processing unit and nodes energy.

In WSNs, a sensor node generates, transmits and relays signal among neighbors. For those somewhat "simple" sensors that merely capture temperature, pressure, the energy consumed on data gathering is minor and the transmission energy is dominant in energy consumption. Conversely, the "complex" visual sensors, such as, video surveillance sensors, which are deployed in open areas, for example, shopping malls, airports, national parks and campuses, need relatively higher power for data gathering, analysis and codec. In WVSNs, visual sensors also encode and trans-code the raw video data captured by their visual facility. Specifically, visual nodes can capture video signal; encode or trans-code the raw video to mpeg2/4 video clips; aggregate the duplicated videos; and send them to the cluster heads or the base station. Consequently, the energy consumed by visual nodes is comparatively higher than the sensors without visual facility and energy consumed by wireless communication is not the only dominant energy consumption any more. In some conventional sensor networks, the sensors have continuous power supply and wired communication. However, in the wide-open outdoor areas, it is unrealistic and luxurious to connect the sensors with power and communication cables. Namely, only limited bandwidth and energy can be used by each wireless battery-powered visual node. Like the other WSNs, the limited energy capacity and wireless bandwidth are also the overriding constraints of WVSNs. We provide two approaches, one is reducing the number of transmission video packets and decrease the wireless transmission distance by applying the layered clustering model with video data aggregation, the other is promoting the energy capacity of system by applying rechargeable solar cell to the WVSNs.

3.2   System Setup

The heterogeneous Solar-Powered WVSNs (SPWVSNs) investigated in this thesis has three kinds of sensor nodes, visual sensor nodes, cluster head nodes, and base stations.

The energy capacities of sensor nodes are corresponding to the functions they possessed. Some sensors, such as base stations powered by wall outlet have almost limitless energy capacity; the cluster head nodes have a bigger size solar panel and higher energy capacity; other normal visual sensors recharged by a smaller solar panel have lower energy capacities. The visual sensors, cluster heads and base station are dispersed in several layers; each layer has a number of clusters; each cluster has only one cluster head.

The functions of cluster heads are relaying, encoding, trans-coding and aggregating the raw video data received from visual sensors in its cluster. The number of normal visual sensors in each cluster is proportional to the area of the cluster. The functions of normal visual sensors are generating and sending the raw video data. In our model, the normal visual sensors are only one hop to the cluster heads; the normal visual sensors do not relay the video signals among the neighbors. Furthermore, by applying rechargeable solar cell to the system, solar panel can recharge the sensor cell in daytime when it is not at the maximum energy capacity and the battery overcharging is not detected. For the visual nodes powered by solar cell, when the battery capacity is higher than the energy requirement of visual data generation and transmission, nodes can initialize themselves, capture or send the video signals.

We compare the results in terms of total video packets sent by all the visual nodes with the different cluster numbers in each layer. After applying the layered clustering and solar cell to the WVSNs under the consideration of video quality, we validate that system lifetime is prolonged and performance is improved. In this section, we illustrate the system model that applied in the solar-powered WVSNs. The system model includes solar cell unit, event trigger unit, energy consumption unit, layered clustering unit, and video distortion unit. The definition of system performance evaluation is also given.
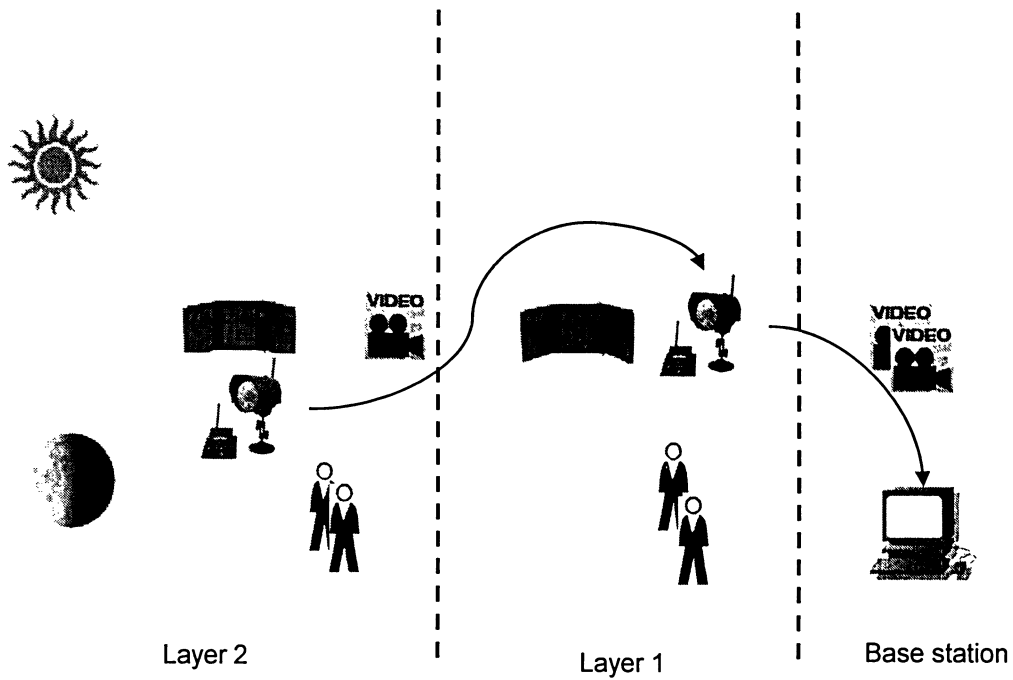
Figure 3.1 Solar-Powered Layered Clustering Wireless Visual Sensor Networks

These five units and definition are employed to formulate the system model and evaluate the performance improvement of SPWVSNs in the following sub-sections. In SPWVSNs, the energy required by wireless transmission from sender to receiver is exponentially proportional to the distance between two nodes [65]. By assigning the network into several segments, a hierarchical network topology can significantly reduce the transmission distance between the distant nodes [10][16]. Hence, the system can significantly reduce the energy exhausted on the long distance transmission by maintaining a hierarchical network structure. In a layered clustering system, the cluster heads take more responsibility. Besides the energy consumed on the long distance wireless communication among cluster heads and base station, the cluster heads also need additional energy in generating video data, trans-coding and aggregating the video data that received from the normal visual sensors in its cluster. Consequently, the cluster head usually requests a higher energy capacity than the normal visual sensors. In the layered

clustering system, normal visual nodes only capture raw video data and send to the cluster heads. This negates the need to relay or send the video data to some distant nodes or the need to encode the video data. Therefore, energy consumption is saved for energy constrained normal visual sensors, which extends the lifetime of the WVSNs in full-scale. The layered clustering SPWVSN is illustrated in Figure 3.1.

3.2.1 Solar Cell Unit

Raghunathan *et al.* developed a prototype of wireless embedded micro-systems that are powered by the solar cell [5]. Our solar cell unit is derived from the system of Raghunathan. The detection of false termination in solar cell charging procedure comes from [3]. The charging power rate at the conditions of outdoor bright sunlight and indoor illumination comes from [4]. On [6], it shows the daytime of the different cities that are located all over the world. In this thesis, we analyze the system performance with the daytime table of Toronto.

For the autonomous solar-powered node, the direct light on the solar panel can only recharge solar cell in daytime. We list the daytime lengths of several cities in Table 3.1 and make use of daytime table of Toronto in the simulation. In Toronto area, the regular shortest daytime is from 07:48 to 18:14; the daytime length (T_s) is 10:26 hours a day. We also assume that full activity time of the WVSNs is daytime, and the solar cell can be recharged by solar panel that directly faces sun in daytime. During T_s, the solar panel recharges solar energy (E_s) into the solar cell. In the other time, since the illumination intensity of light is minor, E_s can be regarded as zero.

Location	Sunrise	Sunset	Daytime length (hours)
Toronto	07:48	18:14	10:26
Los Angeles	07:09	18:04	10:55
Shanghai	06:07	17:09	11:02
London	06:46	16:42	9:56
Tokyo	06:26	16:29	10:03
Berlin	07:43	16:03	8:20
Sydney	06:57	17:06	10:09

Table 3.1 Daytime Table

Solar illumination can yield around $1\,\text{mW/mm}^2$ ($1\,\text{J/day/mm}^2$) in full sunlight or $1\,\mu\text{W/mm}^2$ under bright indoor illumination and the solar cells are about 10-12% efficient [4]. For autonomous solar-powered wireless visual sensor, the total recharged solar energy (E_s) is the product of the solar cells efficiency, the solar illumination, the size of solar panel, and the recharging time. For normal solar-powered visual sensors, we assume that the sizes of the solar panel are equal. In our experiment, the sensors are scattered in an outdoor environment. Hence, the indoor bright situation is not considered in the equation. Equation (1) illustrates the solar cell recharging function for the solar-powered visual sensor.

$$E_s = \begin{cases} \tau \cdot \rho_d \cdot S \cdot \Delta t, & \forall E < E_0, \quad \forall \Delta t \in T_s \\ 0, & others \end{cases} \tag{1}$$

If the energy recharged by solar panel (E_s) is specified, solar panel size (S) can be worked out from equation. Table 3.2 lists parameters used in the equation (1).

Parameter	Description
$\tau = 10\%$	Solar cell efficiency
$\rho_d = 1 \text{ mW/mm}^2$	Solar illumination in daytime
$T_s = 10{:}26$ hours	Daytime

Table 3.2 Solar Function Parameters

3.2.2 Event Trigger Unit

Yong *et al.* provided an event trigger unit for heterogeneous sensor networks [17]. First, an independent packet streams with Poisson distribution in the clustering sensor network is given. Then, according to probability theory, the expectations of total packets generated by sensor nodes are calculated. In this thesis, we revise the energy functions by adopting the event trigger unit.

A static WVSN can be modeled as $S(N_i, W_i)$, where N_i is the set of visual sensors and W_i is the set of directed wireless links from the sensors to the cluster heads. In this thesis, we assume that the visual sensors only capture and transmit the raw video data to the cluster heads, do not relay the data among the normal visual sensors. The cluster heads in outskirt layer receive, encode, aggregate the raw video data and send the encoded data to the cluster heads in the inner layer. The cluster heads in the inner layer receive, trans-code, aggregate the video data from the visual nodes in their clusters; and relay the encoded data from the cluster heads in the outskirt layer to the base station.

Given an example, N visual nodes are randomly spread in an area with L layers. Layer i has C_i clusters and one cluster head in each cluster; each cluster has N_{vi} normal visual sensors that only connect their cluster heads directly; C_1 layer 1 cluster heads connect base station ($N_b = 1$). Therefore, the total nodes number of a two layers SPWVSN can be

represented in equation (2). Table 3.3 lists the descriptions of the parameters in equation (2).

$$N = C_1 \cdot (N_{v1} + 1) + C_2 \cdot (N_{v2} + 1) + 1 \qquad (2)$$

Parameter	Description
i	i-th layer
C_i	Number of clusters in i-th layer
N_{vi}	Number of normal visual sensors in each i-th layer cluster
N_b	Number of base station

Table 3.3 Nodes Number Parameters

In this work, we assume that in layer i, the cluster head i communicates with N_{vi} visual sensor nodes. Further, all the visual sensors in cluster i have identical independent packet streams with Poisson distribution [17], the video packets for cluster head i are also Poisson process. Denote λ_j as the packets generated by visual node j and λ_{ch} as the packets generated by cluster head. If all packet generation rates of visual nodes in cluster i are same ($\forall \lambda_j = \lambda_{ch} = \lambda$), the cluster head's video packet arrival rate function is denoted as follows,

$$\lambda_i = \lambda_{ch} + \sum_{j=1}^{N_v} \lambda_j = (N_v + 1)\lambda, \quad \forall \lambda_j = \lambda_{ch} = \lambda \qquad (3)$$

According to probability theory, the expectation value of a visual node is λt and the expectation value of a cluster head's video arrival packets $X_i(t)$ is

$$\overline{X_i(t)} = (N_v + 1)\lambda t, \quad \forall \lambda_j = \lambda_{ch} = \lambda \qquad (4)$$

3.2.3 Energy Consumption Unit

In terms of an energy consumption function, let E_n be the energy of a visual sensor, which is composed of three parts: energy consumption of transmission (E_t), energy recharged by solar panel (E_s), and energy consumption of video processing (E_v). The energy consumption of solar-powered visual node is illustrated in Figure 3.2. The procedure starts from a visual node with maximum energy capacity. Each time when an event is triggered, the visual node checks its energy capacity. If it is higher than the required energy of processing action, the visual node can capture, generate visual packets and send them to the cluster head. If the time slot between two events is in daytime, the solar panel will recharge the energy into the solar cell. If the overcharging of the solar cell is detected, the energy capacity of the visual node will keep at maximum energy capacity (E_0). If not, the energy capacity of the sensor is the sum of E_{n-1} and E_s, then minus E_t and E_v. If the time slot is not in daytime, E_s can be neglected. The sensor energy is deducted by E_t and E_v. Equation (5) is the energy function of solar-powered visual sensor in WVSN.

$$E_n = \begin{cases} E_{n-1} - E_t - E_v + E_s, & \forall t \in T_s, \quad \forall 0 < E_{n-1} < E_0 \\ E_0, & \forall t \in T_s, \quad \forall E_{n-1} \geq E_0 \\ E_{n-1} - E_t - E_v, & \forall t \notin T_s, \quad \forall 0 < E_{n-1} < E_0 \\ 0, & \forall t \notin T_s, \quad \forall E_{n-1} \leq 0 \end{cases} \qquad (5)$$

It is well known that transmission energy is the sum of the sending energy (E_{ts}) and the receiving energy (E_{tr}), $E_t = E_{ts} + E_{tr}$. E_{ts} is proportional to the n-th power of the distance between the visual nodes and their cluster heads, as shown in equation (6) [34]. The parameter n is the path loss exponent.

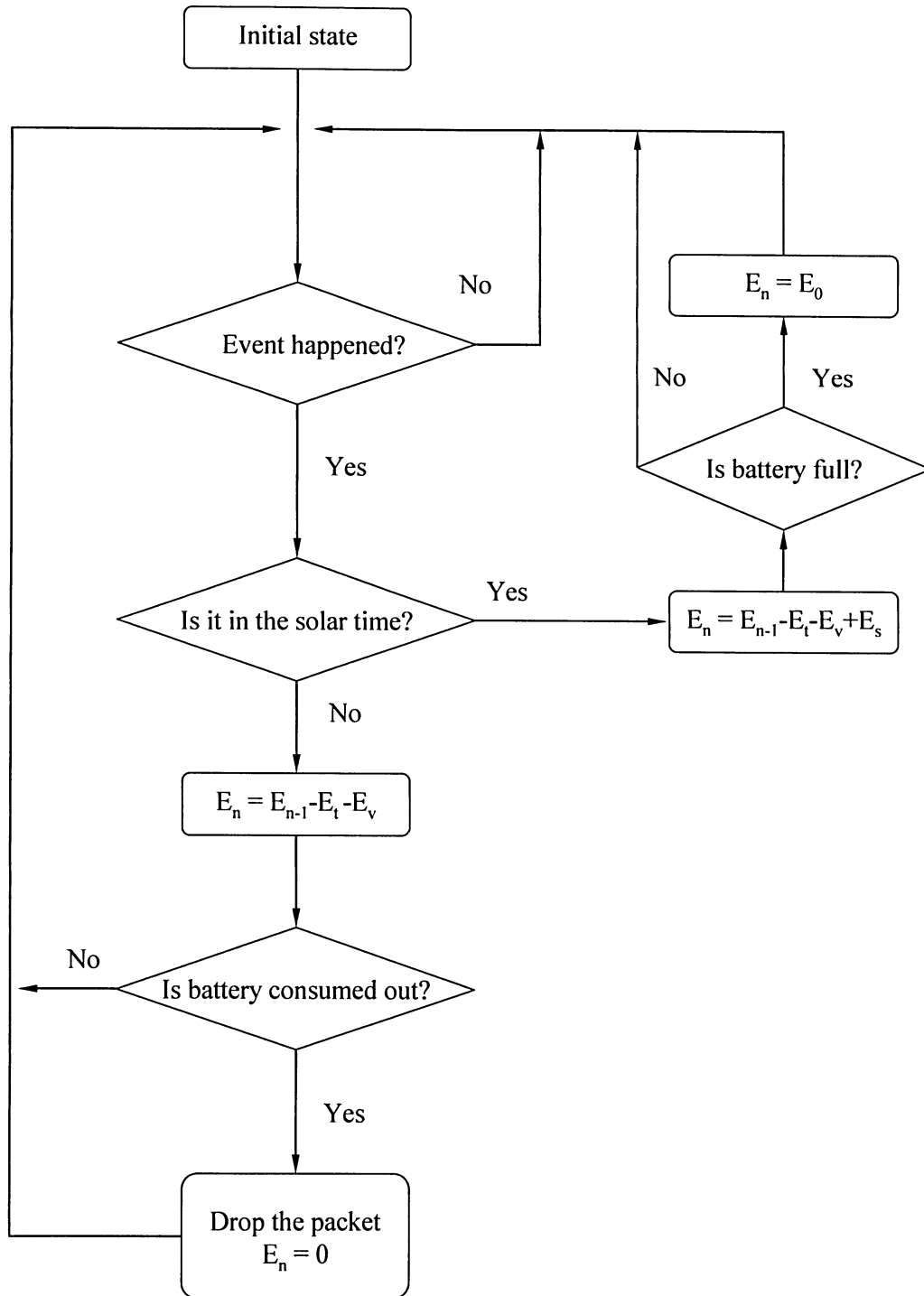$$E_{ts} = \beta + \mu d^n, \quad \forall n \in \{2,3,4,5\} \qquad (6)$$

30

Figure 3.2 Power Consumption of Solar-Powered Wireless Visual Sensor

With sufficiently large time t, the actual event number occurred is very close to its expectation value. Thus, this expectation value is used to calculate the sending energy consumption of visual nodes and cluster heads. The sending energy consumption of a visual node during t is $(\beta + \mu d^n) \cdot \lambda t$. The cluster heads aggregate data received from the visual nodes, then send it out. The aggregation parameter (α) varies from 0 to 1, where 0 means that all packets received by the cluster heads have been dropped; 1 means that all the packets received by the cluster heads will be send out without any aggregation. Thus, the sending energy of a cluster head during t is represented in equation (7).

$$
\begin{aligned}
E_{ts} &= \alpha \cdot (\beta + \mu d^n) \cdot \overline{X_i(t)} = \alpha \cdot (\beta + \mu d^n) \cdot (N_v + 1)\lambda t \\
&\forall n \in \{2,3,4,5\}, \\
&\forall \lambda_j = \lambda_{ch} = \lambda
\end{aligned}
\tag{7}
$$

3.2.4 Layered Clustering Unit

The energy functions of the heterogeneous wireless sensors and an unequal layered clustering model are given in [22]. The wireless sensors are deployed in a wireless sensor network that is composed of a various number of clusters and several layers. The radiuses of the layers are calculated out by the energy functions of cluster heads in the different layers. However, the energy functions do not include the energy consumption of video processing and the energy recharged by solar panel. Moreover, the system's lifetime is also calculated based on the non-rechargeable battery. We modify the energy function of the layered clustering model by adding a renewable energy supply and video processing energy consumption. Thus, we convert the energy function of the wireless sensors to the energy function of solar-powered visual sensors. The system performance is evaluated by total transmitted packets of the WVSNs.

Both equal and unequal layered clustering models of WSNs are discussed in [22]. In the equal layered clustering model, the areas of all clusters are equal. Because the number of nodes in a cluster is proportional to area of the cluster, each cluster in the equal layered clustering algorithm has the same number of nodes. In unequal layered clustering model, the radiuses of inner layer relate to the energy consumption of cluster heads in all layers. The energy consumption of the cluster heads includes the energy consumption of transmission and video processing. We assume that all the cluster heads are identical and have the same initial energy value. In an ideal condition, each cluster head consumes the same amount of energy in a set time ($E_{ch1} = E_{ch2} = \ldots = E_{chi}$). The energy consumption of the cluster heads in layer 2 (E_{ch2}) includes the energy consumption of encoding, aggregating, and trans-coding the raw video data received from all the nodes in the clusters; the energy consumption of capturing video data; the energy consumption of transmitting data from the cluster heads in layer 2 to the cluster heads in layer 1. In this work, the aggregation rate can vary from 0 to 1. For example, if the aggregation rate is 0.1, which means that every 10 packets received by the cluster heads, only 1 packet will be sent out after aggregation. For layer 1 cluster heads, the energy consumption includes the energy consumption of receiving, aggregating and trans-coding the video data received from all the nodes in the clusters; the energy consumption of relaying the video data from the cluster heads in layer 2; the energy consumption of capturing video data; and the energy consumption of transmitting data from the cluster heads in layer 1 to base station.

In our solar-powered wireless visual sensor network, we modify the energy functions of the cluster heads in the layer 1 and 2 by adding the video processing energy (E_v), which is composed of encoding energy (E_{ve}) and capturing energy (E_{vc}), and transform to new energy equations, which are listed in Table 3.4.

Layer 1	Layer 2
$E_{ch1} = E_{t1} + E_{v1} = E_{ts1} + E_{tr1} + E_{v1}$	$E_{ch2} = E_{t2} + E_{v2} = E_{ts2} + E_{tr2} + E_{v2}$
$E_{ts1} = \alpha \cdot \left(\beta + \mu d_1^{\ n}\right) \cdot \left(N_{v1} + N_{v2} + 2\right) \cdot \lambda t$	$E_{ts2} = \alpha \cdot \left(\beta + \mu d_2^{\ n}\right) \cdot \left(N_{v2} + 1\right) \cdot \lambda t$
$E_{tr1} = E_{tr}\left(\alpha N_{v2} + \alpha + N_{v1}\right) \cdot \lambda t$	$E_{tr2} = E_{tr} \cdot N_{v2} \cdot \lambda t$
$E_{v1} = \left(E_{ve}\left(N_{v1} + 1\right) + E_{vc}\right) \cdot \lambda t$	$E_{v2} = \left(E_{ve} \cdot \left(N_{v2} + 1\right) + E_{vc}\right) \cdot \lambda t$
$\forall N_{v1} = \dfrac{R_1^2}{C_1 R_2^2} N_v$	$\forall N_{v2} = \dfrac{R_2^2 - R_1^2}{C_2 R_2^2} N_v$
$\forall n \in \{2,3,4,5\}$	$\forall n \in \{2,3,4,5\}$
$\forall \lambda_j = \lambda_{ch} = \lambda$	$\forall \lambda_j = \lambda_{ch} = \lambda$

Table 3.4 Layered Clustering Equations

3.2.5 Video Distortion Unit

Several video distortion models that are based on Power-Rate model have been developed [34][36][64]. The Power-Rate-Distortion (P-R-D) model is given in the performance analysis of WVSNs. The authors also demonstrate the solution to allocate

resource when the visual quality is at Achievable Minimum Distortion (AMD) in WVSNs. The different simulation results are illustrated when the distortion rate of visual quality varies.

In the experiment, we apply the Power-Rate-Distortion [34][64] to evaluate the lifetime and performance of SPWVSNs when the distortion rate is at AMD (Achievable Minimum Distortion). The equation of distortion model is given in equation (8). Table 3.5 lists the parameters used in the equation.

$$D = D_s(R_s, E_v) = \sigma^2 e^{-\gamma R_s \bullet g(E_v)} \tag{8}$$

Parameter	Description
$g(E_v) = (E_v)^{2/3}$	Energy consumption model
$E_v \in [0, E_0]$	Energy consumption of video processing
$R_s \geq 0$	Bit rate
$\gamma = 11.54$	Model parameter related to encoding
$\sigma^2 = 350$	Input variance

Table 3.5 Power-Rate-Distortion Parameters

For the cluster heads in layer 2 and layer 1, the distortion function D can be transformed to an equation of R_s and E_v. Moreover, when $E_0, E_{ve}, E_{vc}, \beta, \mu, t, \lambda$ are given, the intermediate parameters R_s and E_v only include the two variables: N_v and d. Table 3.6 shows the Power-Rate-Distortion Equations for the solar-powered wireless visual sensor networks.

Layer 1	Layer 2
$D_1 = D_{s1}(R_{s1}, E_{v1}) = \sigma^2 e^{-\gamma R_{s1} \bullet g(E_{v1})}$ $= D_s(N_{v1}, d_1)$	$D_2 = D_s(R_{s2}, E_{v2}) = \sigma^2 e^{-\gamma R_{s2} \bullet g(E_{v2})}$ $= D_s(N_{v2}, d_2)$
$R_{s1} = \dfrac{E_0 - E_{v1}}{\beta + \mu d_1^{\,n}}$	$R_{s2} = \dfrac{E_0 - E_{v2}}{\beta + \mu d_2^{\,n}}$
$E_{v1} = \left(E_{ve}(N_{v1} + 1) + E_{vc} \right) \cdot \lambda t$	$E_{v2} = \left(E_{ve} \cdot (N_{v2} + 1) + E_{vc} \right) \cdot \lambda t$
$E_{v1} \in [0, E_0]$	$E_{v2} \in [0, E_0]$
$\forall n \in \{2,3,4,5\}$	$\forall n \in \{2,3,4,5\}$
$\forall \lambda_j = \lambda_{ch} = \lambda$	$\forall \lambda_j = \lambda_{ch} = \lambda$
$\forall N_{v1} = \dfrac{R_1^2}{C_1 R_2^2} N_v$	$\forall N_{v2} = \dfrac{R_2^2 - R_1^2}{C_2 R_2^2} N_v$

Table 3.6 Power-Rate-Distortion Equations

In the experiment, the encoding energy consumption changes in accordance with the different code formats, such as, mpeg2 or mpeg4. Thus, the energy values consumed by video coding are different. Normally, for using mpeg4 codec, we need spend more energy in the video coding than using mpeg2 codec. Thus, the distortion values of the video data are also varied.

3.3   Experiment

3.3.1 Experiment Setup

The network simulation setup is illustrated in Figure 3.3. It is a circle area with 400 meters radius ($R_2 = 400$m) and 100 visual nodes are randomly distributed in the area. The
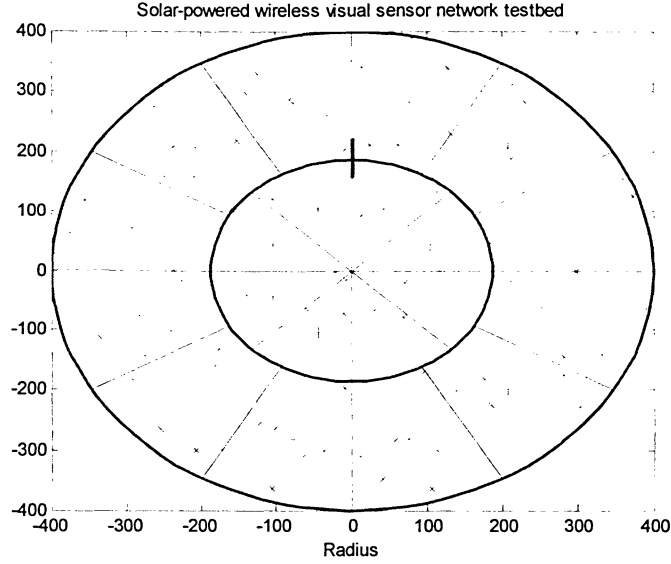
Figure 3.3 Experiment Setup

radius of inner layer (R_1) can be worked out by the system energy equations of E_{ch1} and E_{ch2}. The number (N_{vi}) of visual sensor nodes in each cluster i is proportional to the area of cluster i. Totally, N_v visual sensors are randomly deployed in the round area. In the experiment, we simulate SPWVSN in the area by changing the number of clusters in each layer. The system is composed of 5-20 clusters in layer1 and 6-30 clusters in layer2. Figure 3.3 shows one experiment setup, which includes 8 clusters in layer 1, 12 clusters in layer 2. The red "+" tags represent the cluster heads, the blue "x" tags represent the visual sensors, and the base station is placed in the centre of the area.

3.3.2 Layered Clustering Analysis

There are two kinds of layered clustering algorithms, equal layered clustering and

37

unequal layered clustering in the paper [22]. In order to find the better algorithm for SPWVSNs, we also evaluate both of them in the experiment. After implementing the layered clustering topology in the SPWVSN, we obtain the experimental results by varying cluster numbers in layer 1 and layer 2. The ratios of the nodes number in layer 1 and layer 2 are illustrated in the Figure 3.4. It is evident that the nodes number in layer 1 is always less than that in layer 2. Because layer 1 cluster heads need to relay the video data received from layer 2 cluster heads, the transmission energy consumption of layer 1 cluster heads is much heavier than that of layer 2 cluster heads. Consequently, layer 1 cluster heads can only support fewer nodes in their clusters. Figure 3.4 shows the ratios of the nodes number in layer1 and layer2 when the aggregation rates are 0.1, 0.4, 0.7 and 1. The Y-axis represents the layer 1 cluster number varying from 5 to 20 and the X-axis represents the layer 2 cluster number varying from 6 to 30. As the aggregation rate increases from 0.1 to 1, the range of nodes number ratio decreases from 0.75-0.55 to 0.5-0.2. This is because the layer 1 cluster heads need additional energy to send more packets with the increase of aggregation rate. Consequently, layer 1 cluster heads support fewer nodes in their clusters.

We also compare the energy consumption of the unequal layered clustering model with the equal layered clustering model in Figure 3.5. Figure 3.5 shows the energy ratio of the unequal cluster to the equal cluster as the aggregation rates are 0.1, 0.4, 0.7 and 1. The Y-axis represents the layer 1 cluster number varying from 5 to 20 and the X-axis represents the layer 2 cluster number varying from 6 to 30. As the aggregation rate increases from 0.1 to 1, most of energy consumption ratio of the unequal to equal layered clustering models are always less than 0.8. Specifically, the energy consumption of the unequal layered clustering is always less than the equal layered clustering. From the above simulations, we can conclude that the unequal layered clustering has better performance than the equal layered clustering in energy consumption.
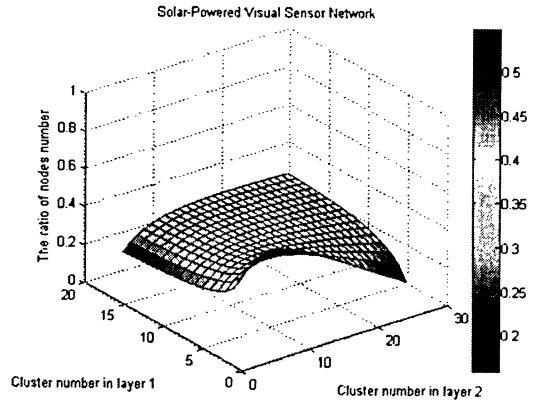
(a) α = 0.1

(b) α = 0.4

(c) α = 0.7
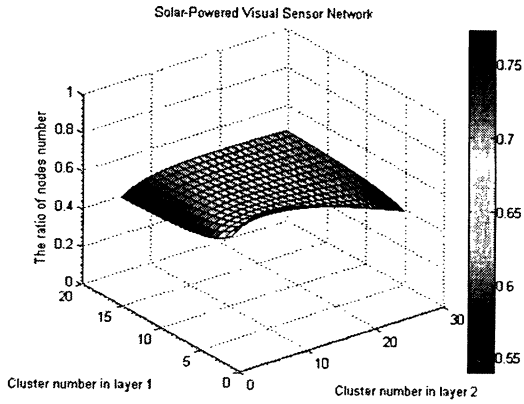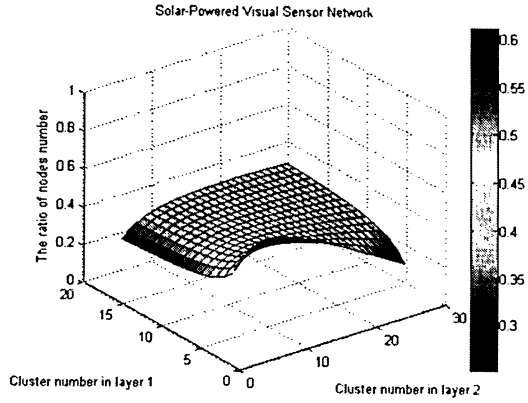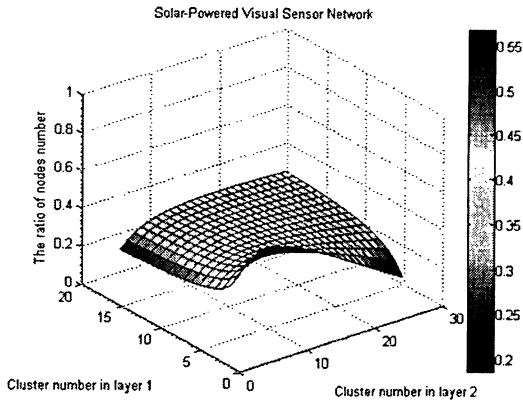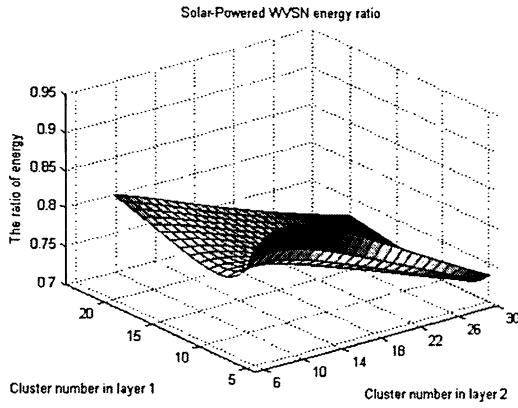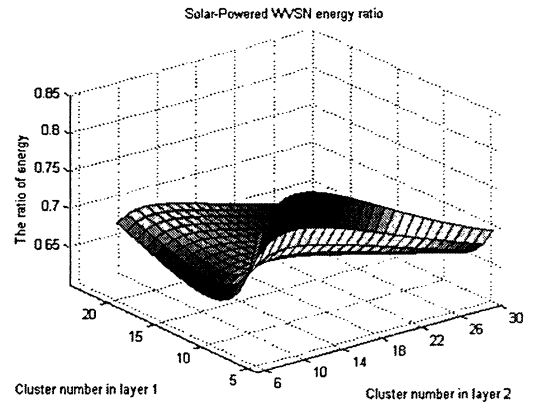
(d) α = 1
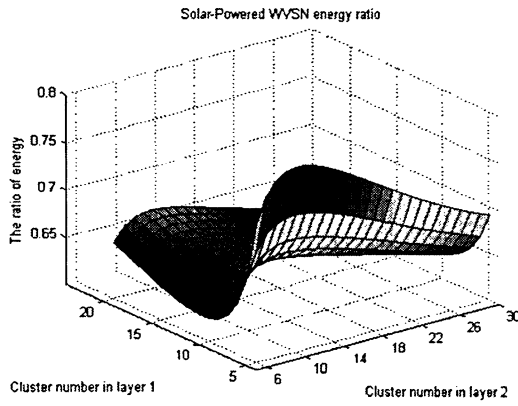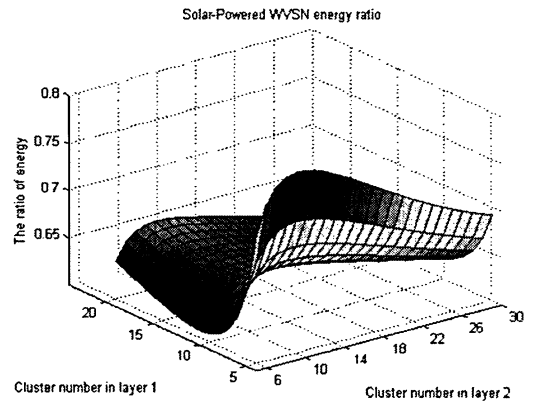
Figure 3.4 Nodes Number Ratio with Different Aggregation Levels

(a) α = 0.1

(b) α = 0.4
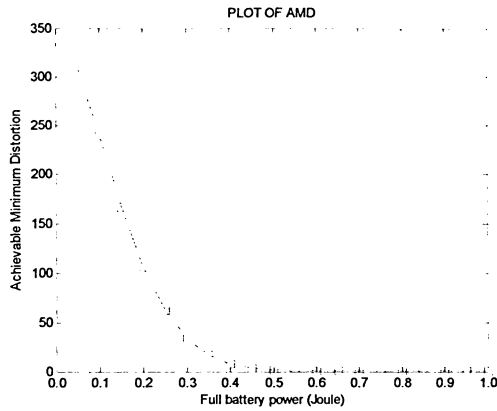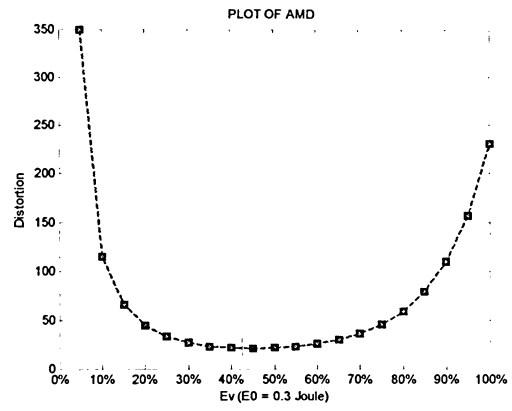
(c) α = 0.7

(d) α = 1

Figure 3.5 Energy Ratio with Different Aggregation Levels

(a) E_0 = 0 - 1.0 Joule   (b) E_0 = 0.3 Joule

Figure 3.6 AMD Analysis

3.3.3 Distortion Rate Analysis

In the experiment, we evaluate the system performance of SPWVSNs by letting the distortion rate at achievable minimum distortion (AMD) of P-R-D model. Figure 3.6(a) is the figure of system minimum distortion values when initial battery energy (E_0) is from 0 to 1.0 Joule. Figure 3.6(b) is the video distortion curve of the system figure when E_0 = 0.3 Joule. It shows the system can reach AMD when the video processing energy (E_v) is about 45% of initial sensor energy (E_0) in our experiment.

Figure 3.7 shows the distortion figures of the WVSNs system as different amounts of clusters in two layers. X-axis is the amount of clusters from 6 to 30 in layer 2, Y-axis is the amount of clusters in layer 1 from 5 to 20 and Z-axis is distortion value. Figure 3.7(a), (b), (c) show the distortion figures when video processing energy (E_v) of visual nodes consumes 10%, 45% and 95% of nodes initial energy (E_0). We observe that the distortion values of nodes are higher when the nodes consume 10% or 95% E_0 in video processing.

41

It is because when the visual nodes spend less energy in video processing ($E_v \downarrow$), the distortion rate is going up ($D \uparrow$); When the visual nodes spend more energy in video processing ($E_v \uparrow$), the energy consumption of transmission is going down ($E_t \downarrow$), the distortion value in transmission is going up ($D \uparrow$). It is easy to conclude that when video processing energy (E_v) of visual nodes takes about 45% E_0, the video quality can reach achievable minimum distortion.

3.3.4 Initial Power Analysis

A normal visual sensor node with a restricted capacitor or battery starts to wake up after the energy level of solar cell reaches GE (Gate Energy), which is the minimum operating energy level for the processor and wireless transmission [66]. However, in WVSNs, initializing sensor modules, capturing raw video and writing to memory require higher energy supply than WSNs without visual functions. The system enforces the sensor to wake up the rest of unit when the energy capacity of the sensor has risen over GE.

In the experiment, we define four GEs (10% E_0, 20% E_0, 30% E_0 and 40% E_0), which is sufficient to power up the visual sensors, capture/encode the raw video data and write to the memory. In Figure 3.8, we set the layer 2 cluster number in X-axis and the layer 1 cluster numbers in Y-axis. From the diagram, the total transmitted packet number keeps higher than the others in most cases when GE is 10% E_0. We can conclude that in the SPWVSNs, the system performance is improved when it has a less GE value.
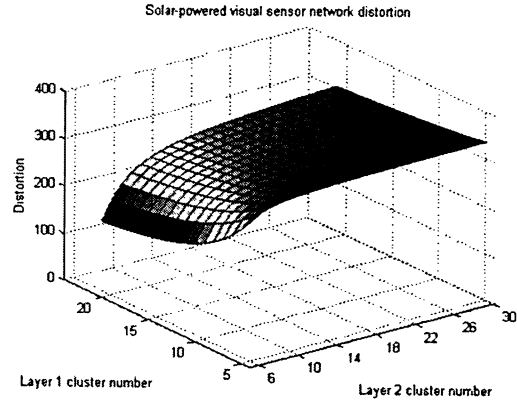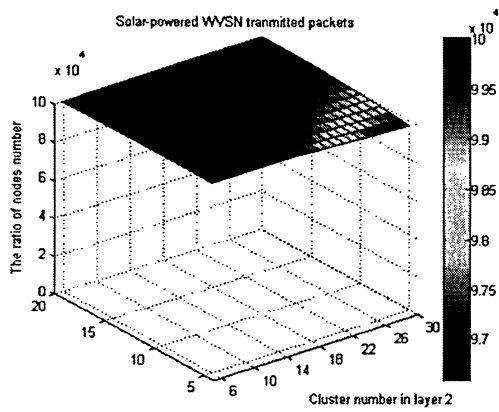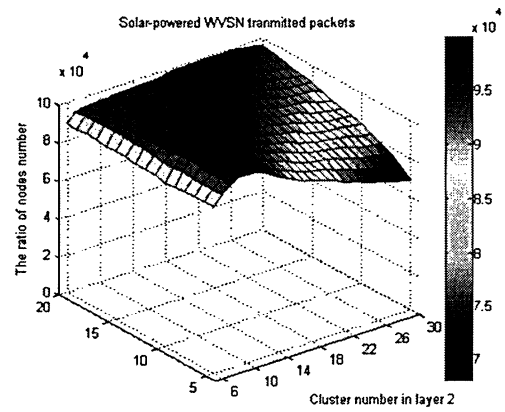
(a) $E_v/E_0 = 10\%$
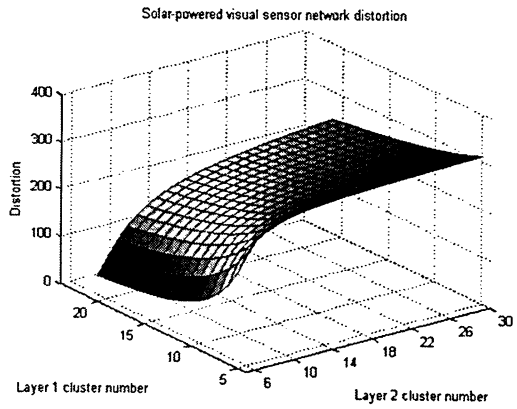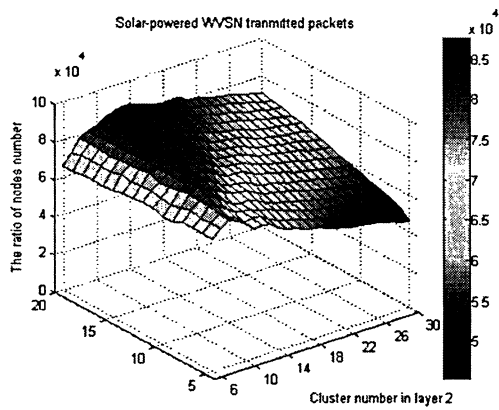

(b) $E_v/E_0 = 45\%$
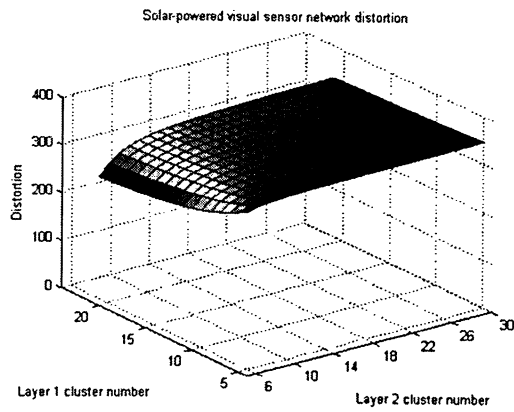
(c) $E_v/E_0 = 95\%$
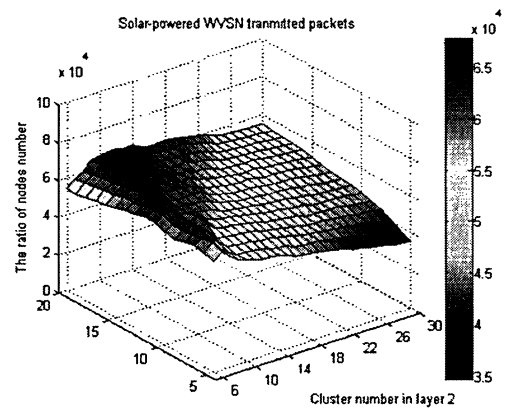
Figure 3.7 Distortion Analysis

GE = 10%E$_0$ GE = 20%E$_0$

GE = 30%E$_0$ GE = 40%E$_0$

Figure 3.8 Total Transmitted Packets with Different GE Values

3.3.5 System Performance Analysis

In some military fields, the standard visual sensors are scattered by airdrop and the energy capacities of these uniform visual sensors are equal. Through experiment, we simulate this situation by randomly generating the locations of all normal visual sensors. For example, in simulation, N visual sensors are randomly distributed in the area. However, for those randomly distributed sensors in each cluster, their distances to the cluster head are different. Usually, visual nodes that are closer to cluster heads need less energy to send the same quantity data than those further away nodes. We simulate this problem by letting transmission energy consumption of each node correspond to the distance from its location to cluster head. Video packets are sent T (T = 1000) times and the T times are randomly selected from 24 hours. It illustrates that each node captures and sends T video packets in one day. At each selected time stamp, the sensor begins to capture video data and transmits one packet, whose size is 15kbits. Because the 100 nodes are randomly scattered in the area, the distances between nodes and cluster heads are different. Correspondingly, the energy consumed by transmitting a video packet varies. In the case of all the normal visual nodes have same initial energy, the remained energy of sensors that are closer to the cluster heads is higher than the further ones after sending the same amount of packets. For each node, if the remained energy of battery or solar cell is less than the energy needed by transmitting packet, it means the energy of node battery has consumed. The sensor thus begins to drop the packets. With solar cell, the sensor can be recharged from solar panel in daytime. During the recharging time, the visual nodes can capture, encode and transmit packets after the battery energy reaches GE. In the experiment, the total number of generated and transmitted packets can be obtained successively. Figure 3.9 shows the total transmitted packets of all the visual nodes in SPWVSNs during one day when the video distortion is at AMD.
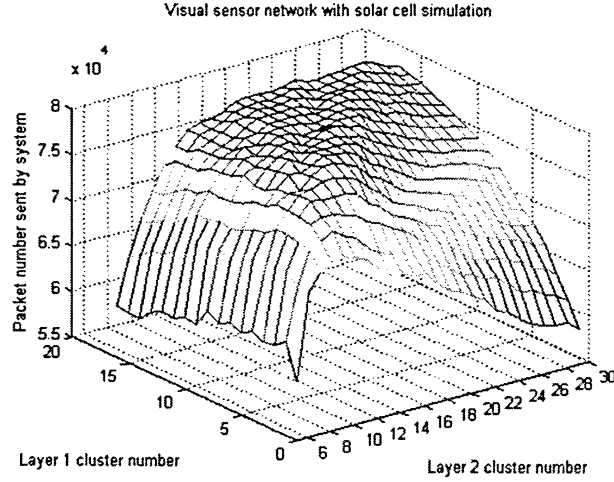
Figure 3.9 Total Transmitted Packets of System

3.4 Summary

In this thesis, we examine the performance of heterogeneous solar-powered WVSNs with the unequal layered clustering model when the video distortion rate is at achievable minimum distortion. When we vary the number of clusters in layer 1 and layer 2, the total energy consumption of all the sensors in the unequal layered clustering model is less than that of the equal layered clustering model in most cases. To sum up, the unequal layered clustering sensor networks prove to be a better solution than the equal layered clustering sensor networks in the sparing energy consumption and enhancing successive delivery rate. Furthermore, we also make the experiment by applying different charging GE values of solar-powered system. The simulation shows that the system may achieve a longer lifetime when it has a less GE value. Through the experiments on our solar-powered dual-layer clustering WVSNs, the system performance can be improved by applying rechargeable solar cell, unequal layered clustering model and a less GE value.

46

CHAPTER 4

VISUAL APPLICATIONS

This chapter first introduces the background knowledge of a post-processing image segmentation technique, PSOTM that can be implemented in the sinks of WVSNs. Then the PSOTM algorithm is presented and the analysis of experimental result are illustrated respectively. The remainder of this chapter is organized as follows,

Section 4.1   introduces the background knowledge PSOTM.

Section 4.2   presents the PSOTM algorithm.

Section 4.3   shows the error measurement, GCE/LCE, which is used in analyzing the experimental result.

Section 4.4   presents PSOTM experimental results of two comparisons, one is the comparison between the SOTM segmentation and PSOTM segmentation, the other is comparison between PSOTM segmentation and manual segmentation.

Section 4.5   summarizes the chapter.

4.1   Background

In WVSNs, we can apply some post-processing techniques, such as image segmentation

and image aggregation to the sink. Because image segmentation demands highly sophisticated algorithms in computational intelligence, image segmentation is usually performed by human beings. However, the high expense and low efficiency of manual work represents the major bottleneck for image segmentations. Segmenting an image in an unsupervised way and improving the efficiency are thus, two major objectives.

Recent research brings forward several suitable self-driven image segmentation techniques that make unsupervised image segmentation possible. Self-Organizing Tree Map (SOTM) is one such unsupervised solution for image segmentation. The SOTM is a special algorithm derived from the Self-Organizing Map (SOM). With the addition of a tree building hierarchy, the SOTM automates the process of determining the correct number of centroids. Furthermore, in image segmentation, the computing method, SOTM, is employed to attain not only the feature points, but also the centre vectors of feature points. It has proved its clustering abilities in performing image segmentation and feature point grouping in the image processing.

The SOTM can be regarded as a mapping from a high dimensional Euclidean space onto a finite set of prototypes. The novel approach has proved to be a potential method to minimize the human beings participation in image processing and automatic segmentation of images. Although the SOTM was extensively studied for minimizing the human beings involvement in image segmentation, SOTM suffers from two constraints. First, it is still a time-consuming approach. Second, the computing hardware demand is relatively high. How can we improve the efficiency of the SOTM while retaining its advantages? At present, SOTM processes tasks in sequence, thus only one SOTM process is running at a time. In this work, we propose parallel SOTM, or PSOTM, to execute multiple SOTM processes in parallel. The major objective of applying PSOTM is to improve the performance efficiency for image processing.

4.2 PSOTM Algorithm

At present, the SOTM processes tasks in sequence, thus only one SOTM process is running at a time. In this thesis, we propose "Parallel Self-Organizing Tree Map (PSOTM)", which aims to improve the processing speed of SOTM. It uses parallel processes to provide a quick segmentation in image processing.

There are two major differences between PSOTM and SOTM. First, PSOTM performs image segmentation in parallel. Precisely, at the beginning of each image segmentation procedure, PSOTM divides the feature points of each image into several clusters, and assigns each cluster to a SOTM process. Therefore, each process only deals with a subset of the original data. At the end of the procedure, the centre points of each cluster are generated by SOTM. PSOTM gathers the results from all the clusters, and generates the final centre points. Secondly, the learning rates [67] in PSOTM are different from those in SOTM. In SOTM, there are two phases in the learning rule, one is the locating phase and the other is the convergence phase. The learning rate is controlled by an adaptation parameter $\alpha(t)$, which decreases with time as weight vectors approach the group centers [46][56]. It generally adapts with a linear function or an exponential function. Thus, $\alpha(t)$ gives a rough weighting, which cannot represent the number of the feature points that have been processed. In PSOTM, the weighting of each centre point is the size of its feature points in the cluster instead of $\alpha(t)$. It represents the weight much more precisely than the adaptation parameter of SOTM.

In the first step of the experiment, the features extracted from the raw image file consist of the Luminance and Chrominance components [68] in HSV domain, and the same values of the image undertake low-pass filters [69] using 3x3 window blocks. Thus, a six-dimension vector is generated for each pixel in the image. To reduce the dimension of the input data, these vectors are pre-processed using Principle Component Analysis (PCA)

[55]. PCA has proved to be a useful statistical technique in face recognition and image compression. The variance of the principle components also can be captured by PCA. Thus, the three-dimensional vectors regenerated from PCA serves as the input data to the PSOTM process.

PSOTM contains the following four stages: stage 1, image pre-processing; stage 2, feature points distribution; stage 3, centre points generation; and stage 4, final centre points generation. In stage 1, the system obtains the feature data by pre-processing the image with a low-pass filter and the Principle Component Analysis (PCA) for reducing the feature dimensions. In stage 2, the system assigns the feature data to several independent processes. In stage 3, each process obtains the centre points and its corresponding weighting factor using the SOTM algorithm. In stage 4, PSOTM collects the results from these independent processes, and generates the final centre points.

Figure 4.1 shows the procedure of image processing by PSOTM algorithm. Initially, 689 feature points have been extracted and are used as the input [70] for three parallel SOTM processes. In stage 1, PSOTM assigns 689 feature points into three clusters. In stage 2, each SOTM processes about 230 feature points in each cluster and obtains 20 centre points. In stage 3, PSOTM collects 60 (20*3) centre points from three clusters. Finally, in stage 4, PSOTM processes these 60 centre points, and generates 10 final centre points.

In Stage 1-2, the neuron update process is denoted in equation (9). c(n) denotes the centre point of the first n feature points, c(n+1) denotes the centre point of (n+1) feature points and v(n+1) denotes the (n+1)-th feature point. Then, c(n+1) is updated by c(n) and v(n+1) as shown in equation (9).
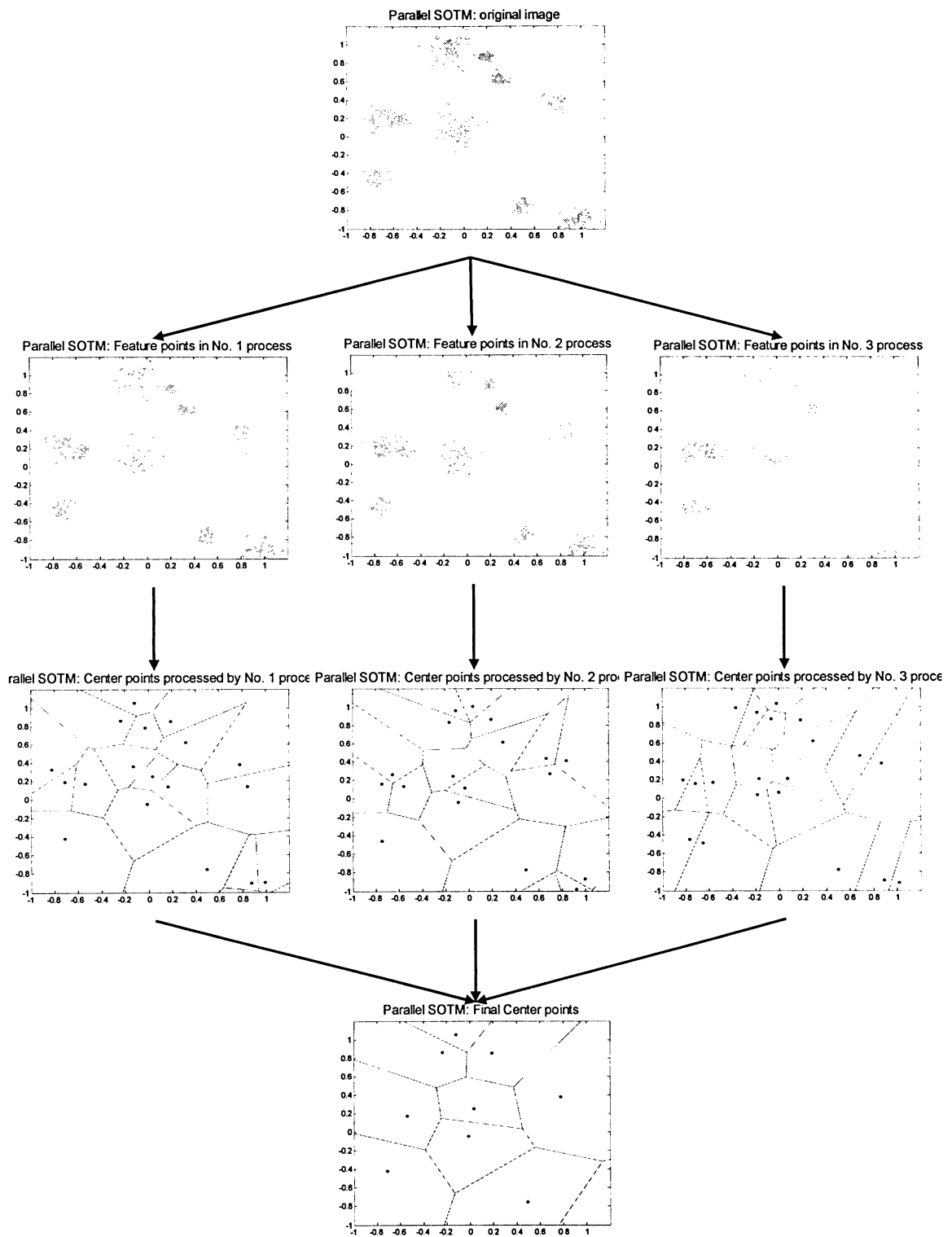
Figure 4.1 PSOTM Procedure

51

$$c(n+1) \quad = \quad \frac{c(n) \cdot n + v(n+1)}{n+1}$$

$$= \quad c(n) + \frac{1}{n+1}[v(n+1) - c(n)] \tag{9}$$

In Figure 4.1, one third of the feature points are assigned into one of three clusters separately. In stage 2, each cluster processes the feature points with SOTM.

The update process in Stage 3-4 can be regarded as a weighted SOTM, and it is expressed in equation (10). c(n+1) denotes the (n+1)-th centre point; $c_{size}(i)$ denotes the size of the i-th centre point; $c_{size}(n+1)$ denotes the size of the (n+1)-th centre point; f(n) denotes the final centre point of the first n centre points and f(n+1) denotes the final centre point of the (n+1) centre points. Therefore, equation (10) shows that f(n+1) is the centre of weighted f(n) and weighted c(n+1).

$$f(n+1) \quad = \quad \frac{f(n) \cdot \sum_{i=1}^{n} c_{size}(i) + c(n+1) \cdot c_{size}(n+1)}{\sum_{i=1}^{n+1} c_{size}(i)}$$

$$= \quad f(n) + \frac{c(n+1) \cdot c_{size}(n+1) - f(n) \cdot c_{size}(n+1)}{\sum_{i=1}^{n+1} c_{size}(i)} \tag{10}$$

$$= \quad f(n) + \frac{c_{size}(n+1)}{\sum_{i=1}^{n+1} c_{size}(i)}[c(n+1) - f(n)]$$

The same algorithm described above can be used for SOTM by setting $c_{size}(i)=1$ in equation (10), which can be simplified as shown in equation (11).

$$f(n+1) \quad = \quad \frac{f(n) \cdot \sum_{i=1}^{n} c_{size}(i) + c(n+1) \cdot c_{size}(n+1)}{\sum_{i=1}^{n+1} c_{size}(i)} \tag{11}$$

$$= \quad \frac{f(n) \cdot n + c(n+1)}{n+1}$$

In stage 3 of Figure 4.1, each cluster generates 20 centres points. Hence, 60 centre points are generated from the three clusters. In stage 4, the system acquires 10 final centre points by processing these 60 centre points with PSOTM algorithm.

Figure 4.2, 4.3 show the pseudo codes of SOTM and PSOTM algorithms. Let d(x,y) denote the Euclidean distance between point x and y. Let H(t) denote the hierarchy control function at iteration t, which determines whether a current centroid will be updated or a new centroid will be created.

4.3   Error Measurement

Even for a same image, human beings perceive different levels of image detail [71]. In order to evaluate the discrepancies between different clustering algorithms, an error measure to quantify the overlapping regions of two segmentation results is required. The error measurements with region differencing are adopted in this experiment. Two precise measurements, Global Consistency Error (GCE) and Local Consistency Error (LCE) [72], are used in this work. These measurements allow labeling refinement in either or both directions.

Let \ and $\|\cdot\|$ denote set difference and cardinality, respectively. Let $R(S, p_i)$ represent the set of pixels corresponding to the region in segmentation S that contains pixel p_i. The local refinement error (LRE) is defined by below equation.

$$LRE(S_1, S_2, p_i) = \frac{\|R(S_1, p_i) \setminus R(S_2, p_i)\|}{\|R(S_1, p_i)\|} \tag{12}$$

The Global Consistency Error (GCE) and Local Consistency Error (LCE) are defined by below equations.

SOTM(feature_point_x, max_iteration, max_centroid)

1. **FOR** each root node of all centroid nodes

2.   **IF** Min(w) > d(feature_point_x, centroid)

3.   **THEN** Min(w) = d(feature_point_x, centroid)

4.   **ENDIF**

5.

6.   **IF** d(x,centroid) < H(t)

7.   **THEN**

8.   winning_centroid = the_reinforced_learning_rule

9.   **ELSE**

10.   new_centroid_node = x

11.   **INCREMENT** Count

12.   **ENDIF**

13.

14.   **IF** Max(d(x,centroid)) > max_distance

15.   **or** iteration > max_iteration

16.   **or** centroid > max_centroid

17.   **THEN**

18.   **RETURN** centroid

19.   **ENDIF**

20. **End FOR**

Figure 4.2 Pseudo Code of the SOTM Algorithm

54

PSOTM(center_point_x, max_iteration, max_centroid)

1. **FOR** each cluster of all clusters

2.   **IF** Min(w) > d(center_point_x, centroid)

3.   **THEN** Min(w) = d(center_point_x, centroid)

4.   **ENDIF**

5.

6.   **IF** d(x,centroid) < H(t)

7.   **THEN**

8.   winning_centroid = the_reinforced_learning_rule

9.   **ELSE**

10.   new_final_centroid_node = x

11.   **INCREMENT** Count

12.   **ENDIF**

13.

14.   **IF** Max(d(x,centroid)) > max_distance

15.   **or** iteration > max_iteration

16.   **or** centroid > max_centroid

17.   **THEN**

18.   **RETURN** final_centroid

19.   **ENDIF**

20. **End FOR**

Figure 4.3 Pseudo Code of the PSOTM Algorithm

1.   **% Define the LRE**

2.   LRE_s1_s2_p = size_original_ image;

3.   LRE_s2_s1_p = size_compared_image;

4.

5.   **% Calculate LRE**

6.   **For** j=1:size_s1

7.   LRE_s1_s2 = difference_original_compared /

      size_row_original;

8.   LRE_s2_s1 = difference_original_compared / size_row_compared;

9.   **End**

10.

11.   **% Calculate GCE and LCE**

12.   GCE = 1/size(s1,2) * min(sum(LRE_s1_s2_p), sum(LRE_s2_s1_p));

13.   LCE = 1/size(s1,2) * sum(min(LRE_s1_s2_p, LRE_s2_s1_p));

Figure 4.4 Pseudo Code of GCE/LCE

$$GCE(S_1,S_2) = \frac{1}{n}\min\left\{\sum_i LRE(S_1,S_2,p_i), \sum_i LRE(S_2,S_1,p_i)\right\} \qquad (13)$$

$$LCE(S_1,S_2) = \frac{1}{n}\sum_i \min\left\{LRE(S_1,S_2,p_i), LRE(S_2,S_1,p_i)\right\} \qquad (14)$$

The GCE/LCE can be interpreted by pseudo code in Figure 4.4.

4.4   Experiment

The computer environment of experiment is made up of one Pentium 4 3.0GHz CPU, 1GB memory, 80 GB hard drive, windows XP operating system, and the simulation

software is MATLAB 7. Two comparison models, one is comparison between the SOTM segmentation and PSOTM segmentation, the other is comparison between the SOTM/PSOTM segmentation and manual segmentation, are employed in the experiment. The system takes around one day to finish the image processing with SOTM algorithm. However, it spends much less time in processing image by PSOTM (N=2...5) algorithm in same computer environment. In the two models' experiments, the error values (GCE/LCE values) of SOTM and PSOTM are always in the same level. Moreover, comparing with SOTM, PSOTM not only improves the efficiency of image processing by increasing the number of parallel processes but also retains a minor impact on the image quality.

4.4.1 SOTM and PSOTM Segmentation

In this comparison model, five experiments are implemented in five setups with different cluster numbers, SOTM (cluster number N=1) and PSOTM (N=2...5). After the image is segmented by the SOTM or PSOTM, we compare the results of each PSOTM (N=2...5) with the result of SOTM (N=1). The results of experiment are measured with GCE and LCE. House image and Ping-Pong image are processed by SOTM and PSOTM in this experiment. Figure 4.5 shows the segmentation results of the House image. Figure 4.5(a) is the original image, Figure 4.5(b) is generated by SOTM, and Figure 4.5(c,d,e,f) are generated by PSOTM with SOTM cluster number N=2 to 5 respectively. Comparing with original image, Figure 4.5(b), processed by SOTM, becomes less detailed, but more clear-cut. The visual qualities of Figure 4.5(c,d,e,f), which are generated by PSOTM (N=2...5), are comparable with the quality of Figure 4.5(b). The walls and shadow of the house, the trees around the house are almost the same. In the experiment, the effect of parallel SOTM on the image quality is limited. However, there are also some differences

between Figure 4.5(b) and Figure 4.5(c,d,e,f). Several detail points are only showed in Figure 4.5(c,d,e,f), and the frames of the windows in Figure 4.5(c,d,e,f) are much clearer than those in Figure 4.5(b). In Table 4.1, GCE and LCE values of PSOTM (N=2...5) are in the same level, varying from 0.1 to 0.2. The increments of GCE and LCE values are not proportional to the number of processes in the PSOTM.

PSOTM	N=2	N=3	N=4	N=5
LCE	0.15	0.15	0.1	0.18
GCE	0.16	0.16	0.12	0.2

Table 4.1 GCE/LCE Values of House Image

The other image used in the experiment is Ping-Pong image. Figure 4.6(a) is the original image. Figure 4.6(b,c,d,e,f) are results generated by SOTM and PSOTM (N=2...5) respectively. Since the Ping-Pong image has less detail and simple content, we observe insignificant differences between the results of SOTM and PSOTM. The GCE and LCE values of N (N=2...5) parallel SOTM are also showed in Table 4.2. All the GCE/LCE values of experiment are in the limited range of 0.0124-0.0408. After comparing the GCE/LCE values, it is easy to conclude that the error ranges between the image segmentation results of different parallel processes and SOTM are in the same level. The increments of GCE and LCE values are not proportional to the number of processes in the PSOTM.

PSOTM	N=2	N=3	N=4	N=5
LCE	0.0124	0.0221	0.0340	0.0325
GCE	0.0170	0.0291	0.0408	0.0356

Table 4.2 GCE/LCE Values of Ping-Pong Image
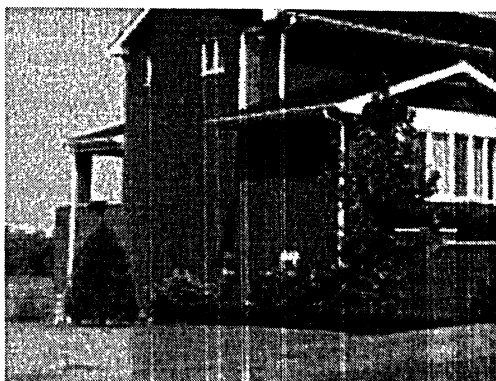
(a) Original

(b) SOTM (*N*=1)

(c) PSOTM (*N*=2)

(d) PSOTM (*N*=3)

(e) PSOTM (*N*=4)

(f) PSOTM (*N*=5)

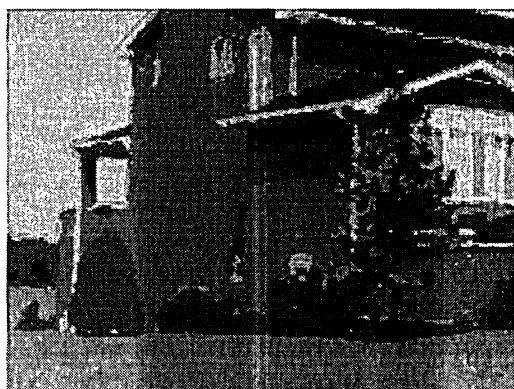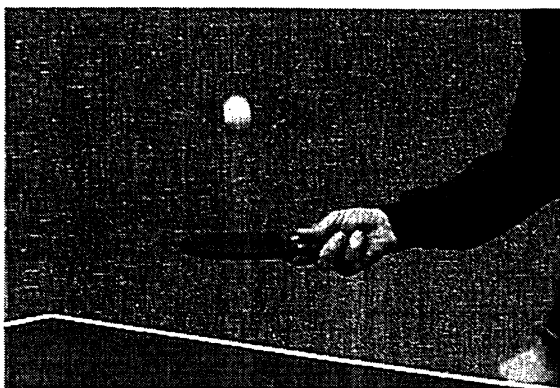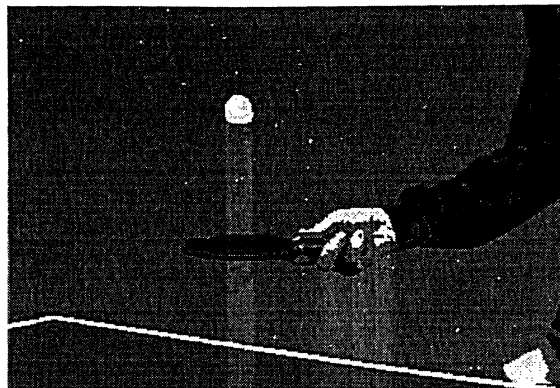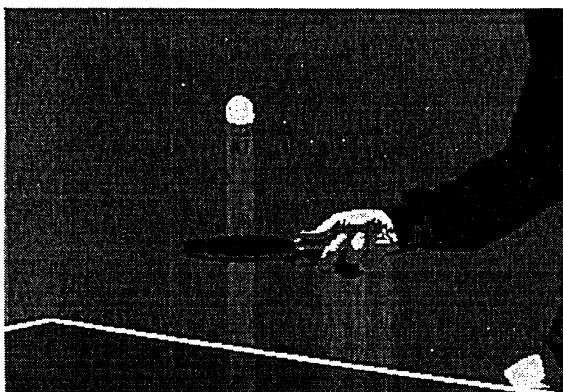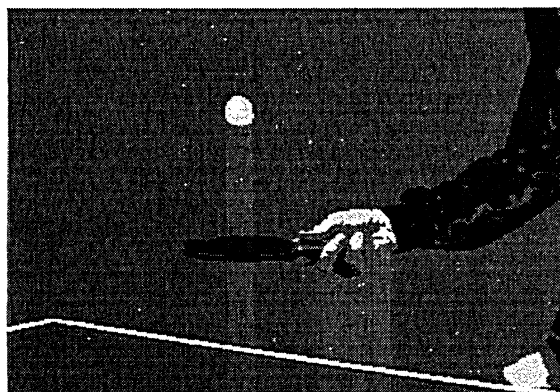Figure 4.5 Segmentation Results for House Image

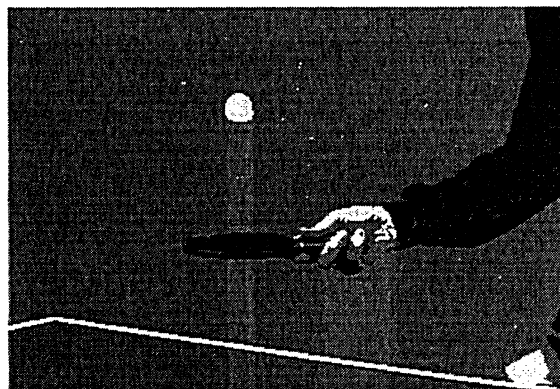(a) Original

(b) SOTM (N=1)

(c) PSOTM (N=2)

(d) PSOTM (N=3)

(e) PSOTM (N=4)

(f) PSOTM (N=5)

Figure 4.6 Segmentation Results for Ping-Pong Image

60

4.4.2 SOTM/PSOTM and Manual Segmentation

In this subsection, the experiment is built on the comparison between the unsupervised image segmentation and manual image segmentation. We use the image dataset from Berkeley University [73][74]. In the manual segmentation file of the dataset, the segmentation part has four columns: the first is segmentation number, followed with row number, start column number, end column number. The segmentation file ends with ".seg". The overall structure of the file is shown in the Figure 4.7 [73][74].

The file is begun with the header, which is mainly ascii text. The comments can also be included in the head. The comments are begun with a character, '#'. The header is separated from the data with a line containing the literal text "data". The header can contain the following information, in any order. The {width, height, segments} lines are required. Others are optional. In the data line, we can use '*' to be the default value. The format of the data section of the file is described in the format line. 'ascii cr' (cr = compressed row) is the default and recommended format. The other formats are superfluous. Each line in the data section contains 4 integers, $<s>$ $<r>$ $<c1>$ $<c2>$, and all values start counting at 0.

Variable	Description
$<s>$	Segment number
$<r>$	Row number
$<c1>$	Leftmost column number of the segment
$<c2>$	Rightmost column number of the segment

Table 4.3 Segment File Variables

1.	\<header\>	
2.	format {*ascii|binary} {*cr|map}	
3.	date \<date string\>	
4.	image \<int\>	# image ID number
5.	user \<int\>	# user ID number
6.	width \<int\>	# width of image
7.	height \<int\>	# height of image
8.	segments \<int\>	# number of segments
9.	gray {*0|1}	# image presented in grayscale?
10.	invert {*0|1}	# image presented with pixel values
11.		# inverted?
12.	flipflop {*0|1}	# image presented upside-down and
13.		# backwards?
14.	\</header\>	
15.	\<data\>	
16.	\<s\> \<r\> \<c1\> \<c2\>	
17.	\</data\>	
18.	\<end\>	

Figure 4.7 Manual Segment File Format

The line means that columns [\<c1\>..\<c2\>] of row \<r\> belong to segment \<s\>. Lines of this sort can appear in any order, and can be reordered with no harm. The only rule is that each pixel must be named only once.

At the beginning of the experiment, a manual segment image is generated by filling up the image with the segment id (id=1 to m) from the leftmost column to rightmost column of each segment. Thus, this manual segment image shows the segments with the segment number from 1 to m. Figure 4.8 and Figure 4.9 show 6 manual segment images.

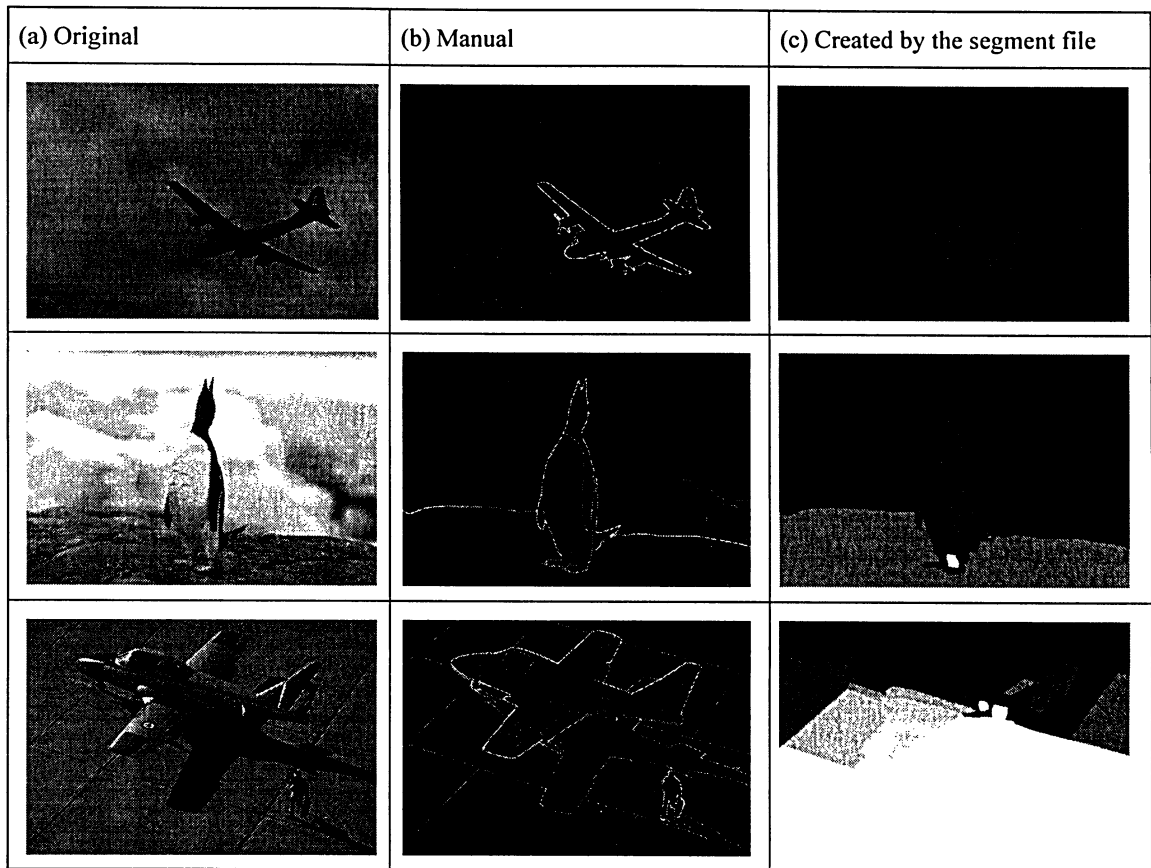| (a) Original	(b) Manual	(c) Created by the segment file

Figure 4.8 Manual Segment Images

The original images are showed in Column (a); the manual segment images are showed in Column (b); the images created by the segment files are showed in Column (c).

Then, we use two manual segment images: Church image and Eagle image. Each image compares with its SOTM/PSOTM segment image respectively. In the manual segment file of Church image, the segment number is 13. The manual segment image is created with segment id from 1 to 13. Figure 4.10(a) is the original image, Figure 4.10(b) shows the manual segment image and the images processed by SOTM/PSOTM are listed in Figure 4.10(c,d,e,f,g). The error values (GCE/LCE) of comparison between SOTM/PSOTM segment and the manual segment of Church image are showed in Table 4.4.
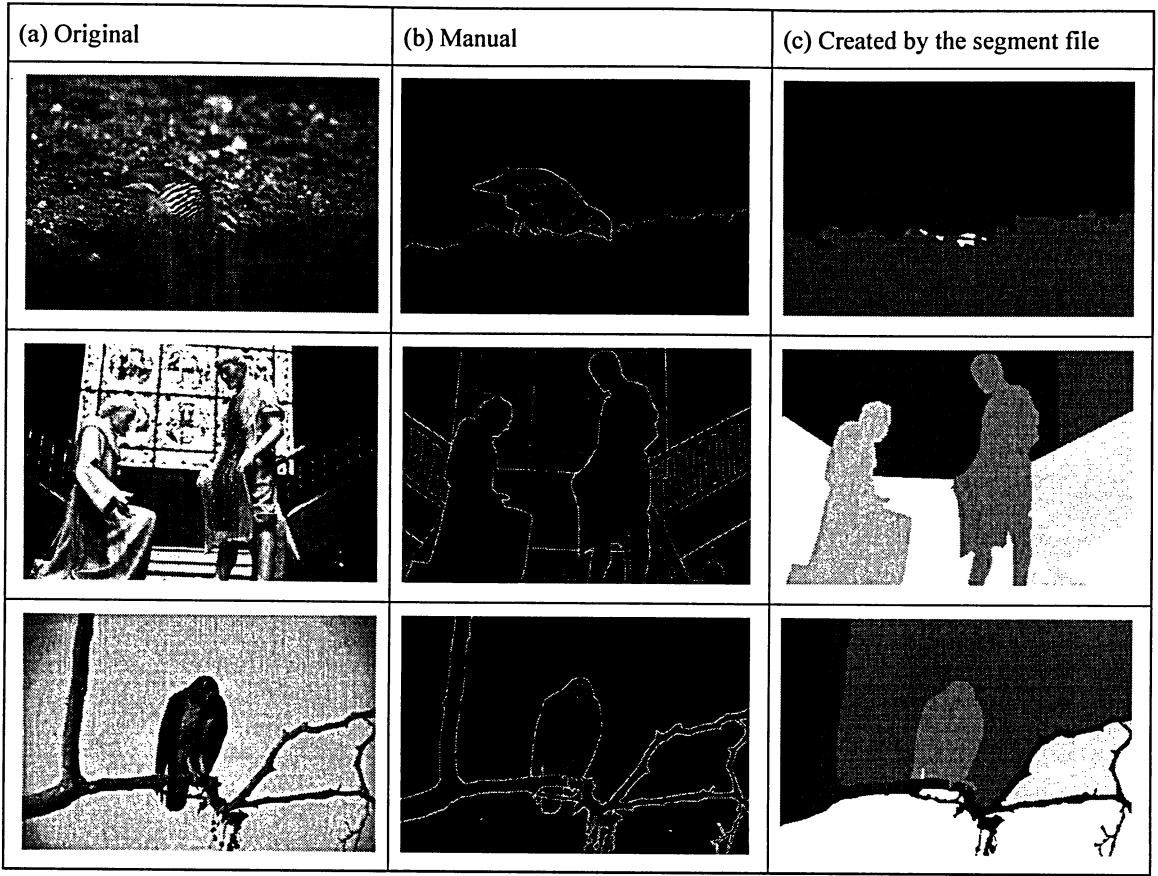
(a) Original	(b) Manual	(c) Created by the segment file

Figure 4.9 Manual Segment Images

PSOTM	N=1	N=2	N=3	N=4	N=5
LCE	0.13	0.12	0.14	0.14	0.14
GCE	0.15	0.14	0.17	0.17	0.17

Table 4.4 GCE/LCE Values of Church Image

For Eagle image, its segment number is 5. The manual segment image is generated with segment id from 1 to 5. Figure 4.11(a) is original image; Figure 4.11(b) is the manual segment image; and the images processed by SOTM/PSOTM are showed in the Figure 4.11(c,d,e,f,g). The error values (GCE/LCE) of comparison between SOTM/PSOTM segment and the manual segment of Eagle image are in Table 4.5.
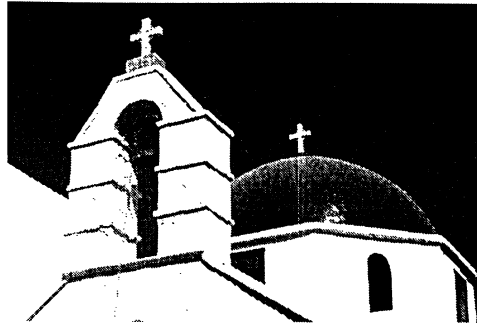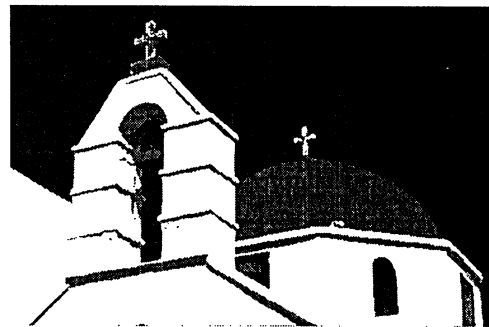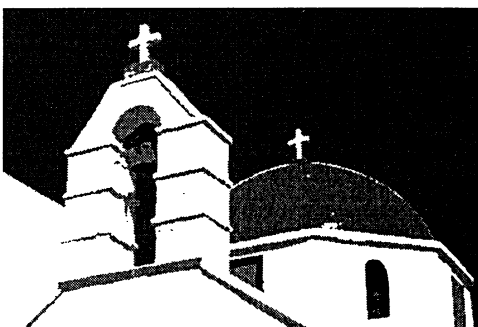
(a) Original
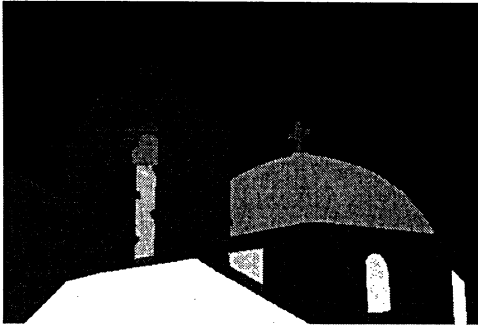
(b) Manual
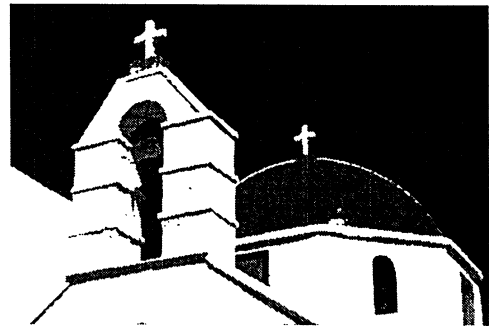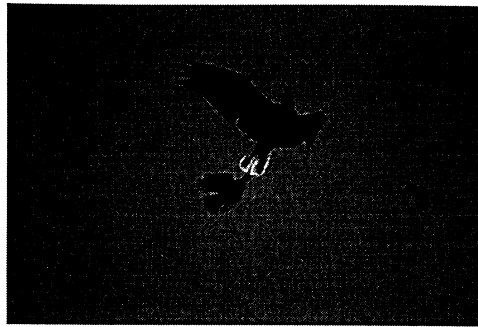
(c) SOTM (N=1)

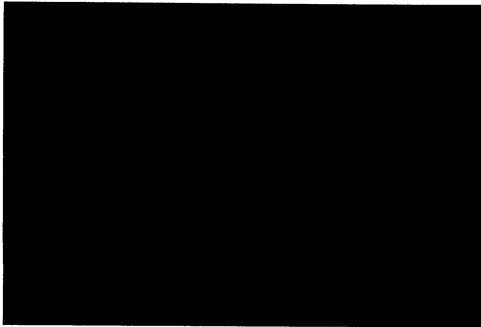(d) PSOTM (N=2)

(e) PSOTM (N=3)
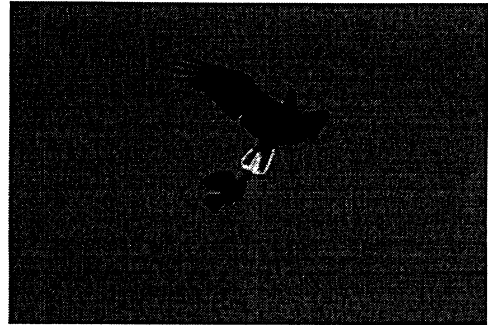
(f) PSOTM (N=4)

(g) Parallel SOTM (N=5)

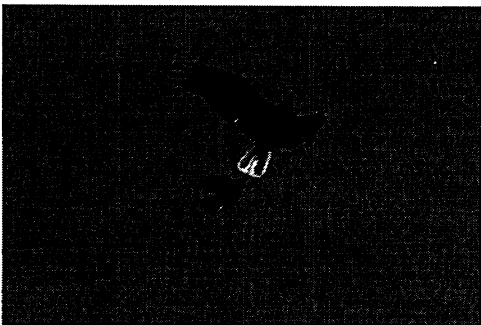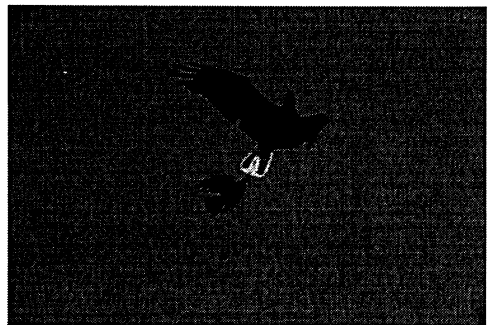Figure 4.10 Segmentation Results for Church Image

(a) Original

(b) Manual

(c) SOTM (N=1)

(d) PSOTM (N=2)

(e) PSOTM (N=3)

(f) PSOTM (N=4)

(g) Parallel SOTM (N=5)

Figure 4.11 Segmentation Results for Eagle Image

PSOTM	N=1	N=2	N=3	N=4	N=5
LCE	0.044	0.037	0.055	0.039	0.044
GCE	0.046	0.041	0.057	0.042	0.047

Table 4.5 GCE/LCE Values of Eagle Image

Table 4.4, 4.5 show the error values (GCE/LCE) of SOTM (N=1)/PSOTM (N=2...5) segmentation compared with the manual segmentation separately. The error measurement (GCE/LCE) values of Church image are in the range of 0.12-0.17 and the error measurement values of Eagle image are in the range of 0.037-0.057. It shows that with the PSOTM method, even the number of SOTM processes increases, the results of image segmentation are always in the same error range. It proves that the image segmentation efficiency can be improved by increasing the number of processes.

Besides the images previous mentioned, some images, such as, animal, boat, human, sports, ocean, island, which have been processed with SOTM/PSOTM are listed in Table 4.6 and 4.7. Their GCE/LCE values of the comparison between the manual segmentation files and SOTM/PSOTM segmentation files are listed under the images. After checking their GCE/LCE values, we found that most of these values are at the same level also.

4.5   Summary

In this work, we proposed a post-processing image technique, PSOTM and examined its performance in segmenting image. PSOTM divides a complex process into multiple independent sub-processes, such that these sub-processes may be computed by multiple machines. Thus, a significant performance gain can be achieved.

We observed that SOTM and PSOTM yield similar segmentation outputs with minor difference. Comparing with manual segmentation results, we observed insignificant

differences between the image segmentations of SOTM and PSOTM. We conclude that the proposed post-processing technique, PSOTM, can reduce the computational time with insignificant impact on the segmentation results.

GCE 0.25-0.28
LCE 0.15-0.19
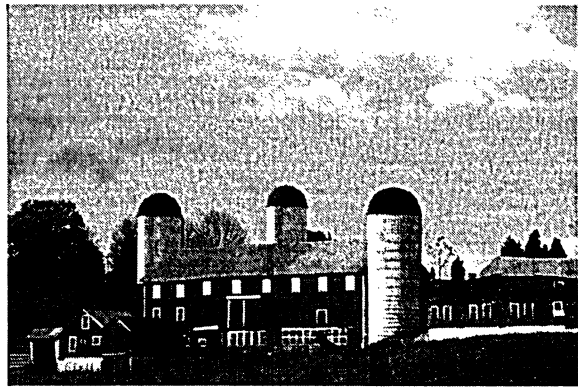
GCE 0.22-0.23
LCE 0.12-0.14
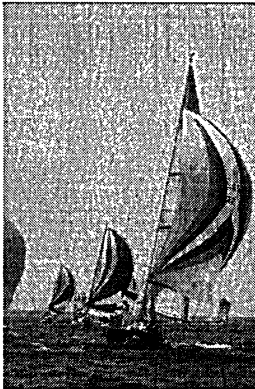
GCE 0.17-0.18
LCE 0.12-0.13

GCE 0.29-0.31
LCE 0.22-0.24

GCE 0.26-0.27
LCE 0.17-0.2

GCE 0.22-0.26
LCE 0.16-0.2

Table 4.6 Segmentation Results for Other Images

GCE 0.21-0.22
LCE 0.16-0.18

GCE 0.12-0.16
LCE 0.11-0.15

GCE 0.037-0.045
LCE 0.03-0.038

GCE 0.12-0.13
LCE 0.076-0.095

GCE 0.17-0.23
LCE 0.1-0.15

GCE 0.045-0.046
LCE 0.04-0.043

Table 4.7 Segmentation Results for Other Images

CHAPTER 5

CONCLUSIONS AND FUTURE WORK

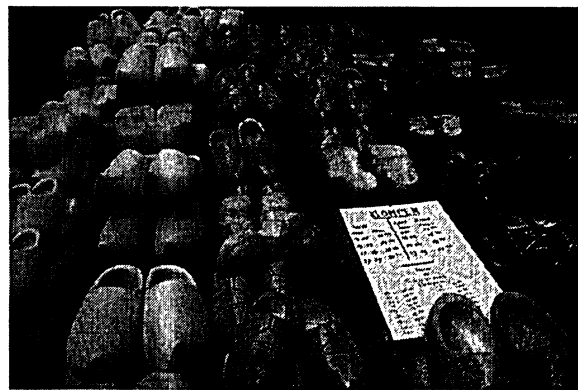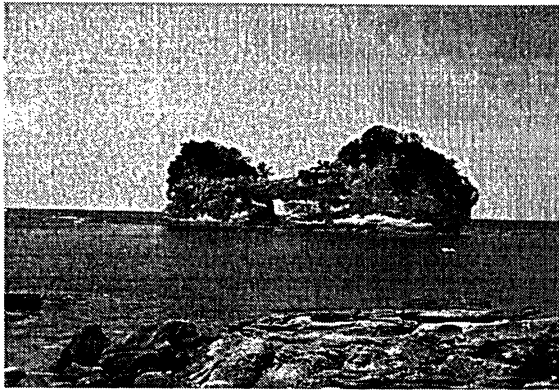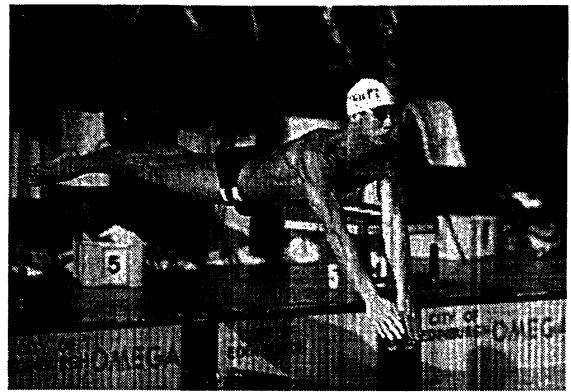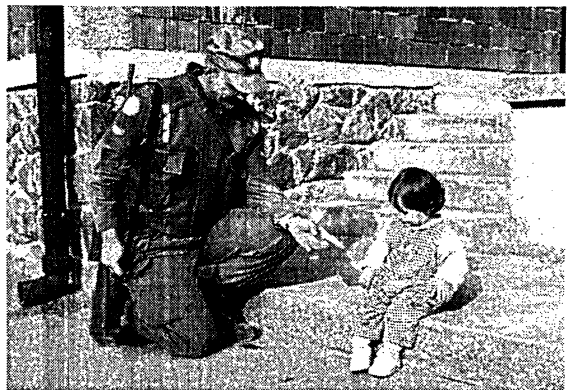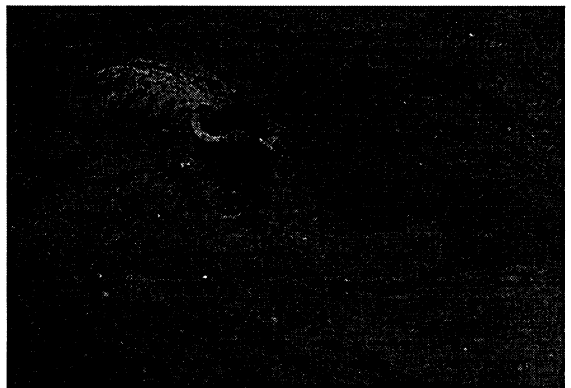This chapter summarizes the work addressed in this thesis, and introduces prospects for future work. We study a solar-powered WVSN and its post-processing image segmentation application, PSOTM.

In WVSNs, due to restricted dimension of the sensor nodes, the limited energy capacity of normal visual sensors is limited. However, energy requirements of their communication and visual facility are much high. Thus, the energy constraint is more critical in WVSNs. By arranging sensors into different layers and clusters, the layered clustering model can dramatically shorten the communication distance. Instead of sending video packets to distant nodes, the layered clustering model lets the sensor nodes only send raw video data to the cluster heads. Then the cluster heads aggregate, and relay the encoded visual data to the base station. The communication energy is thus saved by the shortened distance.

After receiving all the encoded video data from the cluster heads, the sink can process the video data with a post-processing algorithm, PSOTM. Instead of processing the image in series, PSOTM makes use of several parallel SOTM processes in the image segmentation. The experimental result demonstrates that PSOTM improves the efficiency of the image segmentation without significant sacrificing the segmentation performance. The contribution of this thesis is summarized as below:

- We examined the capability of a layered clustering model in transmitting the

71

video data and saving energy consumption among the heterogeneous solar-powered wireless visual sensor nodes when the video data distortion rates are at different values. We applied the rechargeable solar cell module, the energy consumption module, and the event trigger module to the WVSNs. In the visual quality analysis, the Power-Rate-Distortion model was applied to the WVSNs. With the layered clustering model, we analyzed the experimental results of ratio of total nodes in the different layers and the quantity of total transmitted video packets at the different distortion rates. We concluded that the layered clustering model can dramatically increasing the performance of WVSNs in communication and energy consumption.

- A novel post-processing image segmentation algorithm, Parallel Self-Organizing Tree Map (PSOTM), has been proposed to process the image segmentation in the sink. We adopted GCE and LCE as our error measurements, and evaluated the image segmentation result of PSOTM by comparing it with the results of SOTM and the manual image segmentation. Compared to the SOTM image segmentation algorithm and manual image segmentation, PSOTM can process the image in parallel with insignificantly impact on the image segmentation result. We concluded that PSOTM can improve performance in image segmentation.

For the future work, some aspects are worth further investigating, such as:

- In heterogeneous solar-powered WVSNs that are applied with layered clustering algorithm, the energy consumption and the total transmitted packets number could be examined in the scenario when the sensor nodes are mobile.

- In homogeneous solar-powered WVSNs that are applied with layered clustering algorithm, the system lifetime can be prolonged by rotating the cluster heads based on the evaluation of their remained energy. That means the cluster heads are

not static or predefined, and the dynamic cluster heads can be elected periodically by comparing the remained energy.

- We will also focus our research on performance analysis of solar-powered WVSNs under the considerations of the view coverage of visual sensor and error estimation in wireless transmission.

BIBLIOGRAPHY

[1] D. Estrin, D. Culler, K. Pister, and G. Sukatme, "Connecting the physical world with pervasive networks", *IEEE Pervasive Computing*, vol. 1, Issue 1, pp.59-69, Jan.-Mar. 2002.

[2] G. J. Pottie and W.J.Kaiser, "Wireless integrated network sensors", *Communications of the ACM*, vol. 43, Issue 5, pp.51-58, May 2000.

[3] F. Boico, B. Lehman, and K. Shujaee, "Solar Battery Chargers for NiMH Batteries", *Power Electronics Specialists Conference*, pp.146-152, 2005.

[4] B.A. Warneke, M.D. Scott, B.S. Leibowitz, Lixia Zhou, C.L. Bellew, J.A. Chediak, J.M. Kahn, B.E. Boser, and K.S.J. Pister, "An autonomous 16 mm/sup 3/ solar-powered node for distributed wireless sensor networks", *Proceedings of IEEE Sensors*, vol. 2, pp.1510-1515, Jun. 2002.

[5] V. Raghunathan, A. Kansal, J. Hsu, J. Friedman, and M. Srivastava, "Design considerations for solar energy harvesting wireless embedded systems", *International Symposium on Information Processing in Sensor Networks*, pp.457-462, 2005.

[6] http://www.gaisma.com/en/location.

[7] A. Mohan, Wei Hong, D. Gay, P. Buonadonna, and A. Mainwaring, "End-to-end performance characterization of Sensornet multi-hop routing", *International Conference Pervasive Services*, pp.27-36, 2005.

[8] N. Pham Nam, J. Youn, and W. Chulho, "A Comparison of Wireless Sensor Network Routing Protocols on an Experimental Testbed", *IEEE International Conference on Sensor Networks, Ubiquitous, and Trustworthy Computing*, vol. 2, pp.276-281, 2006.

[9] Ooi, C.-C., and N. Fisal, "Implementation of geocast-enhanced AODV-bis routing protocol in MANET", *TENCON*, vol. 2, pp.660-663, 2004.

[10] R. Bai, and M. Singhal, "DOA: DSR over AODV Routing for Mobile Ad Hoc Networks", *IEEE Transactions on Mobile Computing*, vol. 5, Issue 10, pp.1403-1416, Oct. 2006.

[11] Y. Yuasa, M. Bandai, and T. Watanabe, "Routing Protocol of Sustainable Sensor Networks with High Exchangeability of Nodes", *Vehicular Technology Conference*, vol. 2, pp.583-587, 2006.

[12] S. Gwalani, E.M. Belding-Royer, and C.E. Perkins, "AODV-PA: AODV with path accumulation", *IEEE International Conference on Communications*, vol. 1, pp.527-531, 2003.

[13] B. Awerbuch, D. Holmer, H. Rubens, K. Chang, and I.-J. Wang, "The pulse protocol: sensor network routing and power saving", *Military Communications Conference*, vol. 2, pp.662-667, 2004.

[14] K. Zheng, N. Wang, and A. Liu, "A new AODV based clustering routing protocol", *International Conference on Wireless Communications, Networking and Mobile Computing*, vol. 2, pp.728-731, Sept. 2005.

[15] S. Marwaha, K. T. Chen, and D. Srinivasan, "A novel routing protocol using mobile agents and reactive route discovery for ad hoc wireless networks", *IEEE International Conference on Networks*, pp.311-316, Aug. 2002.

[16] K.S. Chan, H. Pishro-Nik, and F. Fekri, "Analysis of hierarchical algorithms for wireless sensor network routing protocols", *IEEE Wireless Communications and Networking Conference*, vol. 3, pp.1830-1835, Mar. 2005.

[17] M. Yong, and J.H. Aylor, "System lifetime optimization for heterogeneous sensor networks with a hub-spoke technology", *IEEE Transactions on Mobile Computing*, vol. 3, pp.286-294, Jul. 2004.

[18] X. Du, and F. Lin, "Improving routing in sensor networks with heterogeneous sensor nodes", *Vehicular Technology Conference*, vol. 4, pp.2528-2532, May 2005.

[19] R. Madan, and S. Lall, "Distributed algorithms for maximum lifetime routing in wireless sensor networks", *IEEE Transactions on Wireless Communications*, vol. 5, Issue 8, pp.2185-2193, Aug. 2006.

[20] D. Vaidya, J. Peng, L. Yang, and J.W. Rozenblit, "A Framework for Sensor Management in Wireless and Heterogeneous Sensor Network", *IEEE International Conference and Workshops on Engineering of Computer-Based Systems*, pp.155-162,

Apr. 2005.

[21] K. Yamasaki, and T. Ohtsuki, "Design of energy-efficient wireless sensor networks with censoring, on-off, and censoring and on-off sensors based on mutual information", *Vehicular Technology Conference*, vol. 2, pp.1312-1316, 2005.

[22] S. Soro, and W.B. Heinzelman, "Prolonging the lifetime of wireless sensor networks via unequal clustering", *Proceedings of IEEE International Parallel and Distributed Processing Symposium*, pp.8, 2005

[23] E. Biagioni, and S. H. Chen, "A reliability layer for ad-hoc wireless sensor network routing", *Proceedings of the 37th Annual Hawaii International Conference on System Sciences*, pp.8, Jan. 2004.

[24] I. Gerasimov, and R. Simon, "A bandwidth-reservation mechanism for on-demand ad hoc path finding", *Proceedings of 35th Annual Simulation Symposium*, pp.27-34, 2002.

[25] Y. Zhang, and T.A. Gulliver, "Quality of service for ad hoc on-demand distance vector routing", *IEEE International Conference on Wireless And Mobile Computing, Networking And Communications*, vol. 3, pp.192-196, Aug. 2005.

[26] V.S. Mansouri, B. Afsari, and H. Shahmansouri, "A Simple Transport Protocol for Wireless Sensor Networks", *Proceedings of International Conference on Intelligent Sensors, Sensor Networks and Information Processing Conference*, pp.127-131, Dec. 2005.

[27] R.C.M. Gomes, J. Kelner, E.J.P. Souto, and D. Sadok, "Evaluating energy mechanisms for routing in wireless sensor networks", *International Conference on Mobile Technology, Applications and Systems*, pp.8, Nov. 2005.

[28] C. Heeseok, P. Ilgon, S. Youngsam, and P. Seungmin, "A design and implementation of wireless sensor network routing on Nano-Qplus platform", *International Conference on Advanced Communication Technology*, vol. 1, pp.3, Feb. 2006.

[29] D. Tian, and N.D. Georganas, "Energy efficient routing with guaranteed delivery in wireless sensor networks", *IEEE Wireless Communications and Networking*, vol. 3, pp.1923-1929, 2003.

[30] C. Tan, and S.K. Bose, "Investigating Power Aware AODV for Efficient Power Routing in MANETs", *International Conference on Information, Communications and Signal Processing*, pp.584-588, Dec. 2005.

[31] J. Kim, and J. Jang, "A performance evaluate of improved AODV-based power-aware routing protocol in MANET", *Proceedings of International Workshop on Enterprise networking and Computing in Healthcare Industry*, pp.273-277, Jun. 2005.

[32] X. Hong, M. Gerla, H. Wang, and L. Clare, "Load balanced, energy-aware communications for Mars sensor networks", *IEEE Aerospace Conference Proceedings*, vol. 3, pp.1109-1115, 2002.

[33] J. Randall, L. Guan, X. Zhang, and W. Li, "Investigations of the self organising tree

map", *Proceedings of International Conference on Neural Information Processing*, Vol. 2, pp.724-728, Nov.1999.

[34] Z. He, and D. Wu, "Resource Allocation and Performance Analysis of Wireless Video Sensors", *IEEE Transactions on Circuits and Systems for Video Technology*, vol. 16, Issue 5, pp.590-599, May 2006.

[35] Z. He, and D. Wu, "Accumulative visual information in wireless video sensor network: definition and analysis", *IEEE International Conference on Communications*, vol. 2, pp.1205-1208, May 2005

[36] Z. He, and S.K. Mitra, "From rate-distortion analysis to resource-distortion analysis", *IEEE Circuits and Systems Magazine*, vol. 5, Issue 3, pp.6-18, 2005.

[37] K. Chow, K. Lui, and E.Y. Lam, "Balancing image quality and energy consumption in visual sensor networks", *International Symposium on Wireless Pervasive Computing*, pp.5, Jan. 2006.

[38] P. Muneesawang, and L. Guan, "Automatic machine interactions for content-based image retrieval using a self-organizing tree map architecture", *IEEE Transactions on Neural Networks*, Vol. 13, Issue 4, pp.821-834, Jul. 2002.

[39] S. W. Kim, "Cooperative relaying architecture for wireless video sensor networks", *International Conference on Wireless Networks, Communications and Mobile Computing*, vol. 2, pp.993-998, Jun. 2005.

[40] K. Obraczka, R. Manduchi, and J.J., Garcia-Luna-Aveces, "Managing the

information flow in visual sensor networks", *International Symposium on Wireless Personal Multimedia Communications*, vol. 3, pp.1177-1181, Oct. 2002.

[41] J. Pan, Hou, Y.T., L. Cai, Y. Shi, and S.X. Shen, "Locating base-stations for video sensor networks", *IEEE Vehicular Technology Conference*, vol. 5, pp.3000-3004, Oct. 2003.

[42] M. Chu, J. Reich, and F. Zhao, "Distributed attention in large scale video sensor networks", *IEE Intelligent Distributed Surveillance Systems*, pp.61-65, Feb. 2004.

[43] Y. Deng, and B. S. Manjunath, "Unsupervised segmentation of color-texture regions in images and video," *IEEE Transactions on Pattern Analysis and Machine Intelligence*, vol. 23, pp.800-810, Aug. 2001.

[44] D. Comaniciu, and P. Meer, "Robust Analysis of Feature Spaces, Color Image Segmentation", *IEEE Computer Society Conference on Computer Vision and Pattern Recognition*, pp.750-755, Jun. 1997.

[45] J. Shi, and J. Malik, "Normalized Cuts and Image Segmentation", *IEEE Transactions on pattern analysis and machine intelligence*, vol. 22, Issue 8, pp.888-905, Aug. 2000.

[46] H. Kong, "Self-Organizing Tree Map and Its Applications in Digital Image Processing", PhD thesis, University of Sydney, 1998.

[47] T. Kohonen, "The self-organizing map", *Proceedings of the IEEE*, vol. 78, Issue 9, pp.1464-1480, Sept. 1990.

[48] J. Vesanto, and E. Alhoniemi, "Clustering of the self-organizing map", *IEEE Transactions on Neural Networks*, vol. 11, Issue 3, pp.586-600, May 2000.

[49] M. Dittenbach, D. Merkl, and A. Rauber, "The growing hierarchical self-organizing map", *Proceedings of the IEEE-INNS-ENNS International Joint Conference on Neural Networks*, vol. 6, pp.15-19, Jul. 2000.

[50] Roger Penrose, "The Emperor's New Mind", *Oxford University Press*, 1990.

[51] J. Randall, L. Guan, X. Zhang, and W. Li, "The hierarchical cluster model for image region segmentation", *Proceedings of IEEE International Conference on Multimedia and Expo*, vol. 1, pp.693-696, Aug. 2002.

[52] K. Jarrah, M. Kyan, I. Lee, and L. Guan, "Application of image visual characterization and soft feature selection in content-based image retrieval", *Proceedings of the International Society for Optical Engineering*, Jan. 2006.

[53] M. Kyan, L. Guan, and S. Liss, "Dynamic feature fusion in the self organising tree map-applied to the segmentation of biofilm images", *Proceedings of IEEE International Joint Conference on Neural Networks*, vol. 4, pp.2441-2446, Jul. 2005.

[54] M. Kyan, L. Guan, and S. Liss, "Refining competition in the self-organising tree map for unsupervised biofilm image segmentation", *International Joint Conference on Neural Networks*, vol. 18, Issue 5-6, pp.850-860, Jun. 2005.

[55] I.T. Jolliffe, "Principal Component Analysis", *Springer*, 2nd edition, 2002.

[56] P. Muneesawang, and L. Guan, "Automatic similarity learning using SOTM for

CBIR of the WT/VQ coded images", *Proceedings of International Conference on Image Processing*, vol. 2, pp.749-752, Oct. 2001.

[57] M.I. Brownfield, K. Mehrjoo, A.S. Fayez, and N.J. Davis, IV, "Wireless sensor network energy-adaptive mac protocol", *IEEE Consumer Communications and Networking Conference*, vol. 2, pp.778-782, Jan. 2006

[58] M.J. Miller, and N.H. Vaidya, "A MAC protocol to reduce sensor network energy consumption using a wakeup radio", *IEEE Transactions on Mobile Computing*, vol. 4, Issue 3, pp.228-242, May-June 2005

[59] T. Boscardin, S. Cai, R.X. Gao, and W. Gong, "Energy efficient MAC protocol for condition monitoring sensor networks", *IEEE Conference on Decision and Control*, vol. 2, pp.1496-1501, Dec. 2004

[60] X. Hou, D. Tipper, and S. Wu, "Traffic-aware gossip-based energy conservation for wireless ad hoc and sensor network routing", *IEEE Consumer Communications and Networking Conference*, vol. 1, pp.341-345, Jan. 2006

[61] W. Li, and H. Dai, "Throughput and energy efficiency of sensor networks with multiuser receivers and spatial diversity", *IEEE International Conference on Acoustics, Speech, and Signal Processing*, vol. 3, pp.645-648, Mar. 2005.

[62] Y. Xu, J. Winter, and W. Lee, "Prediction-based strategies for energy saving in object tracking sensor networks", *IEEE International Conference on Mobile Data Management*, pp.346-357, 2004

[63] R.X. Gao, and Z. Fan, "Architectural design of a sensory node controller for optimized energy utilization in sensor networks", *IEEE Transactions on Instrumentation and Measurement*, vol. 55, Issue 2, pp.415-428, Apr. 2006.

[64] Z. Chen, and I. Ahmad, "Power-rate-distortion analysis for wireless video communication under energy constraints", *IEEE Transactions on Circuits and Systems for Video Technology*, vol. 15, Issue 5, pp.645-658, May 2005

[65] T.S. Rappaport, "Wireless Communications: Principles and Practice", *Prentice Hall*, 2002

[66] P. Dutta, J. Hui, J. Jeong, S. Kim, C. Sharp, J. Taneja, G. Tolle, K. Whitehouse, and D. Culler, "Trio: enabling sustainable and scalable outdoor wireless sensor network deployments", *International Conference on Information Processing in Sensor Networks*, pp.407-415, Apr. 2006

[67] H. Kong, L. Guan, and S. Kung, "A self-organizing tree map approach for image segmentation", *International Conference on Signal Processing*, vol. 1, pp.588-591, Aug. 2002.

[68] R. Hsu, M. Abdel-Mottaleb, and A. K. Jain, "Face detection in color images", *IEEE Transactions on Pattern Analysis and Machine Intelligence*, vol. 24, Issue 5, pp.696-706, May 2002.

[69] G. Strang, and T. Nguyen, "Wavelets and Filter Banks", *Wellesley-Cambridge Press*, 1996.

[70] M. Kyan, and L. Guan, *"Local Variance Driven Self-Organization for Unsupervised Clustering"*, *International Conference on Pattern Recognition*, vol. 3, pp.421-424, Aug. 2006.

[71] R.Unnikrishnan, C.Pantofaru, and M. Hebert, *"A Measure for Objective Evaluation of Image Segmentation Algorithms"*, *IEEE Computer Society Conference on Computer Vision and Pattern Recognition*, vol. 3, pp.34-34, Jun. 2005.

[72] D. Martin, *"An Empirical Approach to Grouping and Segmentation"*, Ph.D dissertation, U. C. Berkeley, 2002.

[73] D. Martin, C. Fowlkes, D. Tal, and J. Malik, *"A database of human segmented natural images and its application to evaluating segmentation algorithms and measuring ecological statistics"*, *Proceedings Of IEEE International Conference on Computer Vision*, vol. 2, pp.416-423, Jul. 2001.

[74] D. R. Martin, C. C. Fowlkes, and J. Malik, *"Learning to detect natural image boundaries using local brightness, color, and texture cues"*, *IEEE Transactions on Pattern Analysis and Machine Intelligence*, vol. 26, Issue 5, pp.530-549, May 2004.

[75] K. Romer, and F. Mattern, "The design space of wireless sensor networks", *IEEE Wireless Communications*, Vol. 11, Issue 6, pp.54-61, Dec. 2004.

[76] T. Haenselmann, "Sensornetworks", *GFDL Wireless Sensor Network textbook*, 2006.

[77] S. Hadim, and N. Mohamed, "Middleware: middleware challenges and approaches for wireless sensor networks", *IEEE Distributed Systems Online*, Vol. 7, Issue 3, Mar.

2006.

[78] V. Mhatre, and C. Rosenberg, "Homogeneous vs Heterogeneous Clustered Networks: A Comparative Study", *Proceedings of IEEE International Conference on Communications*, Jun. 2004.

[79] Y. Gu, Y. Tian, and E. Ekici, "Real-Time Multimedia Processing in Video Sensor Networks", *Signal Processing: Image Communication Journal (Elsevier)*, 2006.

[80] M.J. Kyan, L. Guan, M.R. Arnison, and C.J. Cogswell, "Feature extraction of chromosomes from 3-D confocal microscope images", *IEEE Transactions on Biomedical Engineering*, Vol. 48, Issue 11, pp.1306-1318, Nov. 2001.

[81] I.F. Akyildiz, W. Su, Y. Sankarasubramaniam, and E. Cayirci, "A survey on sensor networks", IEEE Communications Magazine, Vol. 40, Issue 8, pp.102-114, Aug. 2002.

[82] A. Nasipuri, and S.R. Das, "On-demand multipath routing for mobile ad hoc networks", Proceedings of International Conference on Computer Communications and Networks, pp.64-70, Oct. 1999.

[83] M.K. Marina, and S.R. Das, "On-demand Multipath Distance Vector Routing in Ad Hoc Networks", Proceedings of IEEE International Conference on Network Protocols, pp.14-23, 2001.

[84] D. Malan, T. Fulford-Jones, M. Welsh, and S. Moulton, "CodeBlue: An Ad Hoc Sensor Network Infrastructure for Emergency Medical Care", *Proceedings of the*

MobiSys 2004 Workshop on Applications of Mobile Embedded Systems, 2004.

[85] G. Koltsidas, S. Karapantazis, G. Theodoridis, and F. Pavlidou, "A Detailed Study of Dynamic Manet On-demand Multipath Routing for Mobile Ad hoc Networks", International Conference on Wireless and Optical Communications Networks, pp.1-5, Jul. 2007.